GEOCHEMICAL ANALYSIS OF THE WOODFORD SHALE, ANADARKO BASIN, OKLAHOMA

by

KAREN McCREIGHT

Presented to the Faculty of the Graduate School of
The University of Texas at Arlington in Partial Fulfillment
of the Requirements
for the Degree of

MASTER OF SCIENCE IN GEOLOGY

THE UNIVERSITY OF TEXAS AT ARLINGTON

May 2014

Acknowledgements

I would like to thank my advisor, Dr. Harry Rowe, for his encouragement and guidance throughout my undergraduate and graduate career. I would like to thank the Texas Bureau of Economic Geology and Marathon Oil Company for providing the cores used in this study. I would also like to thank Nathan Ganser and Michael Neito for their time in assisting me in data collection. I would like to thank my committee members, Dr. Andrew Hunt and Dr. John Wickham, for their support.

I would also like to acknowledge the support provided by my family, and thank them for always encouraging me to succeed. I would specifically like to thank my wonderful fiancé, Shane, for putting up with me through stressful weeks of study.

February 7, 2014

Abstract

GEOCHEMICAL ANALYSIS OF THE WOODFORD SHALE,

ANADARKO BASIN, OKLAHOMA

Karen McCreight, M.S.

The University of Texas at Arlington, 2014

Supervising Professor: Harry Rowe

The Woodford Shale is a dark, siliceous mudstone that was deposited in a rift basin during late Devonian to early Mississippian times. Three drill cores containing the Woodford Shale from the Anadarko Basin, Oklahoma, have been geochemically analyzed using a handheld energy-dispersive x-ray fluorescence instrument. Each core was analyzed at 3- to 4- inch intervals, providing high-resolution chemostratigraphy. Analysis of the following elemental concentrations was performed: Mg, Al, S, Si, P, K, Ti, Ca, Mn, Fe, Mo, Cr, Ni, Cu, Zn, Th, Rb, U, Sr, Zr, and V. Major element geochemistry supports that the Woodford is a siliceous mudstone, with little carbonate input. The relationship between iron and sulfur depicts a high degree of pyritization. A portion of the Woodford Shale appears to be iron-limited with respect to pyrite formation. Trace element enrichment factors and ratios (Ni/Co, V/Cr, and V/(V+Ni)) indicate anoxic or euxinic, oscillating with dysoxic to oxic, bottom water conditions during deposition of the Woodford Shale.

Table of Contents

Acknowledgements iii
Abstract iv
List of Illustrations vi
List of Tables ix
Chapter 1 Introduction 1
Mudrock Research 1
Geologic Research 4
Stratigraphy 9
Chapter 2 Methods 12
Drill Core Information 12
Energy Dispersive X-Ray Fluorescence (ED-XRF) 12
Chapter 3 Methods 15
Shi Randall 4-29H 15
Ridenour 1-20H 25
Teague 1-14H 34
Chapter 4 Discussion 44
Bulk Geochemistry 44
Major Elements 44
Degree of Pyritization 45
Trace Elements 45
Chapter 5 Conclusions 50
References 51
Biographical Information 55

List of Illustrations

Figure 1-1 Map of United States shale plays. Notice the Woodford Shale in West Texas and Oklahoma. (From U.S. Energy Information Administration, 2011) 2

Figure 1-2 Distribution of Woodford Shale production in Oklahoma up to September 2010. The S. Oklahoma Woodford is also known as the Ardmore Woodford (Continental Resources, 2012). 3

Figure 1-3 County Map of Oklahoma. Counties which the cores in this study originate from are outlined in red. Shi Randall 4-29H is located in Grady County (most southern), Ridenour 1-20H is located in Canadian County, and Teague 1-14 is located in Kingfisher County (most northern). 4

Figure 1-4 Southern Oklahoma Aulacogen evolution (Hoffman et al, 1974) 6

Figure 1-5 Late Devonian paleogeographic map (Blakey, 2013) 7

Figure 1-6 Early Mississippian paleogeographic map (Blakey, 2013) 8

Figure 1-7 Map of south-central United States, showing features that existed during the early and middle Paleozoic (Johnson, 1989) 9

Figure 1-8 Paleogeographic map of the base of the Woodford Shale; study area is outlined in red (from Tarr, 1955) 10

Figure 1-9 Generalized stratigraphic column of the Anadarko Basin (from Rose et al, 2004) 11

Figure 3-1 Down-core plot of %Ca, %Al, %Si, and Si/Al for the Shi Randall 4-29H core 16

Figure 3-2 Down-core plot of %Ti, %K, %Mg, %Fe, and %S for the Shi Randall 4-29H core 17

Figure 3-3 Ternary diagram for the Shi Randall 4-29H core; calcium oxide (CaO), alumina (Al_2O_3), and silica (SiO_2) 18

Figure 3-4 Major element cross-plots for the Shi Randall 4-29H core: (A) %Si versus %Al; (B) %Ca versus %Al; (C) %K versus %Al; (D) %P versus %Al; (E) %Ti versus %Al; (F) %Fe versus %Al 19
Figure 3-5 Cross-plot of %Fe *versus* %S for the Shi Randall 4-29H core. 20
Figure 3-6 Down-core plot of the enrichment factors (EF) of Mo, Cr, U, Ni, Zn, and Cu for the Shi Randall 4-29H core 22
Figure 3-7 Down-core plot of EF Mn, Ni/Co, V/Cr, and V/(V+Ni) for the Shi Randall 4-29H core 24
Figure 3-8 Down-core plot of %Ca, %Al, %Si, and Si/Al for the Ridenour 1-20H core 26
Figure 3-9 shows elemental concentrations, in percent weight, of titanium (Ti), potassium (K), magnesium (Mg), iron (Fe), and sulfur (S). Co-variation is observed between Ti and K, as well as Fe and S. General differences in the concentration of these elements appear to generally coincide with the zonations made based on Si, Ca, and Al (fig. 3-8). 26
Figure 3-9 Down-core plot of %Ti, %K, %Mg, %Fe, and %S for the Ridenour 1-20H core 27
Figure 3-10 Ternary diagram for the Ridenour 1-20H core; calcium oxide (CaO), alumina (Al2O3), and silica (SiO2) 28
Figure 3-11 Major element cross-plots for the Shi Randall 4-29H core: (A) %Si *versus* %Al; (B) %Ca *versus* %Al; (C) %K *versus* %Al; (D) %P *versus* %Al; (E) %Ti *versus* %Al; (F) %Fe *versus* %Al 29
Figure 3-12 Cross-plot of %Fe *versus* %S for the Ridenour 1-20H core 30
Figure 3-13 Down-core plot of the enrichment factors (EF) of Mo, Cr, U, Ni, Zn, and Cu for the Shi Randall 4-29H core. 31

Figure 3-14 Down-core plot of EF Mn, Ni/Co, V/Cr, and V/(V+Ni) for the Ridenour 1-20H core 33
Figure 3-15 Down-core plot of %Ca, %Al, %Si, and Si/Al for the Teague 1-14H core..... 35
Figure 3-9 Down-core plot of %Ti, %K, %Mg, %Fe, and %S for the Ridenour 1-20H core 36
Figure 3-17 Ternary diagram for the Teague 1-14H core; calcium oxide (CaO), alumina (Al2O3), and silica (SiO2) 37
Figure 3-18 Major element cross-plots for the Teague 1-14H core: (A) %Si *versus* %Al; (B) %Ca *versus* %Al; (C) %K *versus* %Al; (D) %P *versus* %Al; (E) %Ti *versus* %Al; (F) %Fe *versus* %Al 39
Figure 3-19 Cross-plot of %Fe versus %S for the Teague 1-14H core 40
Figure 3-20 Down-core plot of the enrichment factors (EF) of Mo, Cr, U, Ni, Zn, and Cu for the Teague 1-14H core 41
Figure 3-21 Down-core plot of EF Mn, Ni/Co, V/Cr, and V/(V+Ni) for the Teague 1-14H core 43

List of Tables

Table 2-1 Drill Core Information 12

Table 3-1. Paleoredox condition indicators (from Hatch and Leventhal, 1992; Calvert and Pederson, 1993; Jones and Manning, 1994; Rimmer, 2003) 23

Chapter 1

Introduction

Mudrock Research

Sedimentology and geochemistry of mudrocks has not been comprehensively researched. Only 1-2% of published sedimentology studies focus on mudrocks; however, mudrocks make up approximately two thirds of sedimentary rocks (Alpine et al, 1980; Blatt, 1980; Potter et al, 1980; Schieber and Zimmerle, 1998). Mudrocks are of interest from an academic standpoint because they provide a record of depositional environment, paleoclimate, and paleoceanography (Schieber and Zimmerle, 1998). From an industrial standpoint, mudrocks are of interest because they may serve as source rocks, reservoirs, or seals for hydrocarbons. Black shales, or mudrocks, are characterized by a dark gray to black color and high organic content (Arthur and Sageman, 1994; Piper and Calvert, 2009). The high organic content of these black shales give them great potential as hydrocarbon sources and reservoirs. Recent advancements in drilling and production technology have spurred exploration of black shales in many localities, including the Woodford Shale of Oklahoma and west Texas (Fig. 1-1).

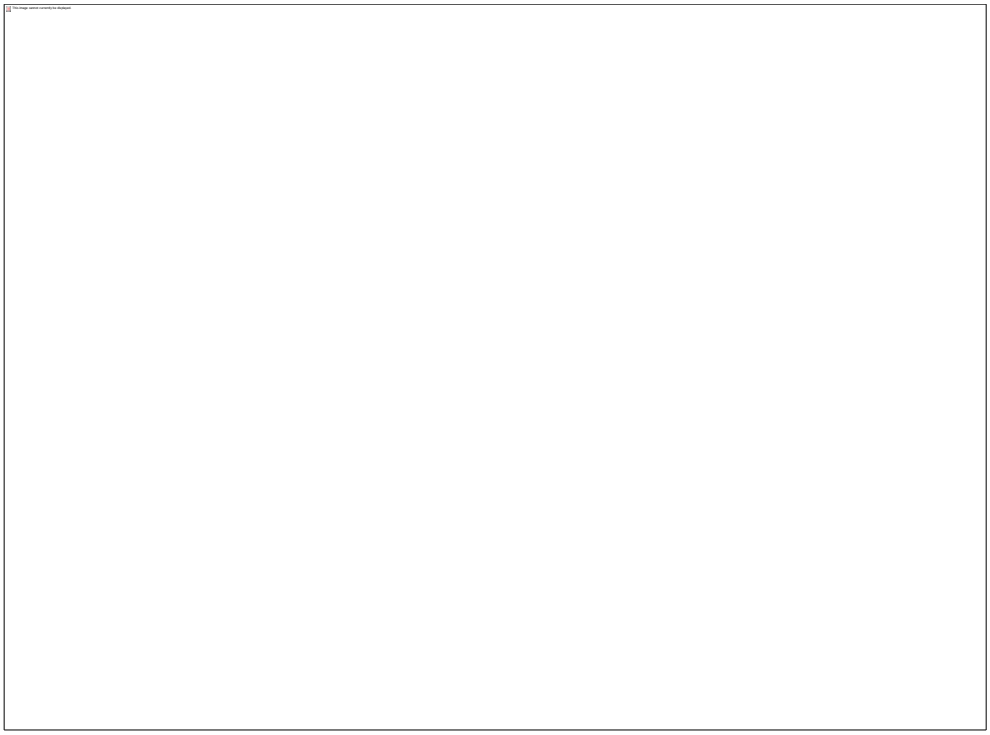

Figure 1-1 Map of United States shale plays. Notice the Woodford Shale in West Texas and Oklahoma. (From U.S. Energy Information Administration, 2011)

The late Devonian to early Mississippian Woodford Shale is an organic-rich, black shale (Hester et al, 1990). The Woodford Shale can be found in west Texas in the Permian and Marfa basins, as well as in Oklahoma in the Arkoma, Ardmore, and Anadarko Basins (Fig. 1-1) (U.S. Energy Information Administration, 2011). The Woodford Shale is most productive in Oklahoma. Between late 2004 and early 2008, the number of wells in the Woodford Shale gas play increased from 24 to over 750 (Vulgamore et al, 2008). In the Arkoma basin, the Woodford Shale is primarily a gas play. As natural gas prices decreased, exploration of the Woodford Shale moved west into the Anadarko and Ardmore basins in hopes of finding oil (Fig. 1-2). Some of the biggest acreage holders in the liquids rich portion of the Woodford Shale play in Oklahoma

include Newfield Exploration, Devon Energy, Marathon oil, Cimarex Energy, ExxonMobil, and PetroQuest Energy (Redden, 2013).

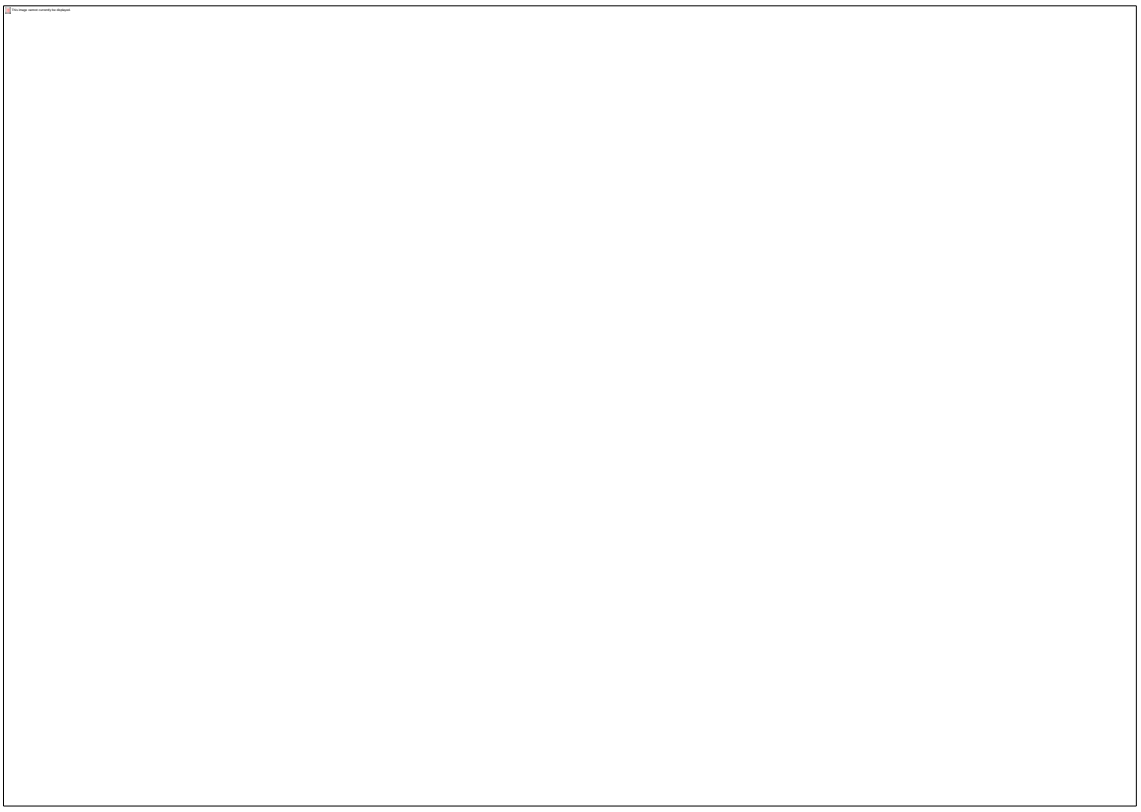

Figure 1-2 Distribution of Woodford Shale production in Oklahoma up to September 2010. The S. Oklahoma Woodford is also known as the Ardmore Woodford (Continental Resources, 2012).

The proposed study focuses on the chemostratigraphy and depositional environment of the Woodford Shale located in the Anadarko Basin. Data from three drill cores will be used in this research project: Shi Randall 4-29H from Grady County, Ridenour 1-20H from Canadian County, and Teague 1-14H from Kingfisher County (Fig. 1-3). The primary objective for collecting geochemical data is to provide a more

comprehensive understanding of the chemical composition of the Woodford Shale of the Anadarko Basin and gain insight into the paleoclimate and paleoceanography.

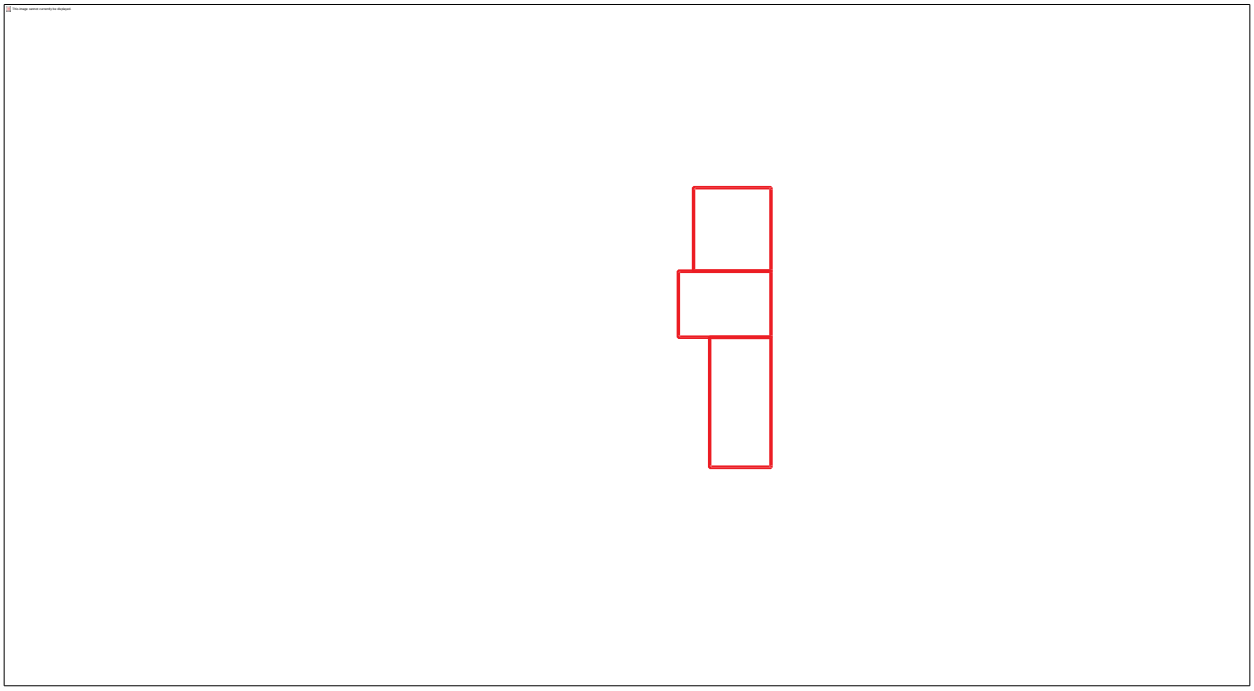

Figure 1-3 County Map of Oklahoma. Counties which the cores in this study originate from are outlined in red. Shi Randall 4-29H is located in Grady County (most southern), Ridenour 1-20H is located in Canadian County, and Teague 1-14 is located in Kingfisher County (most northern).

Geologic Research

Rifting during the Cambrian period formed the Southern Oklahoma Aulacogen (SOA), which was first filled with igneous rocks (fig. 1-4) (Johnson, 1989). Slow subsidence and sediment accumulation occurred in the resulting Oklahoma Basin from late Cambrian to early Mississippian. Sea level fluctuations are evident in depositional cycles in the Arbuckle Group (Franseen et al, 2004) and unconformities in the Hunton

Group (Kuykendall and Fritz, 2001). A significant sea level drop caused an unconformity at the top of the Hunton Group, just below the Woodford Shale (Kuykendall and Fritz,

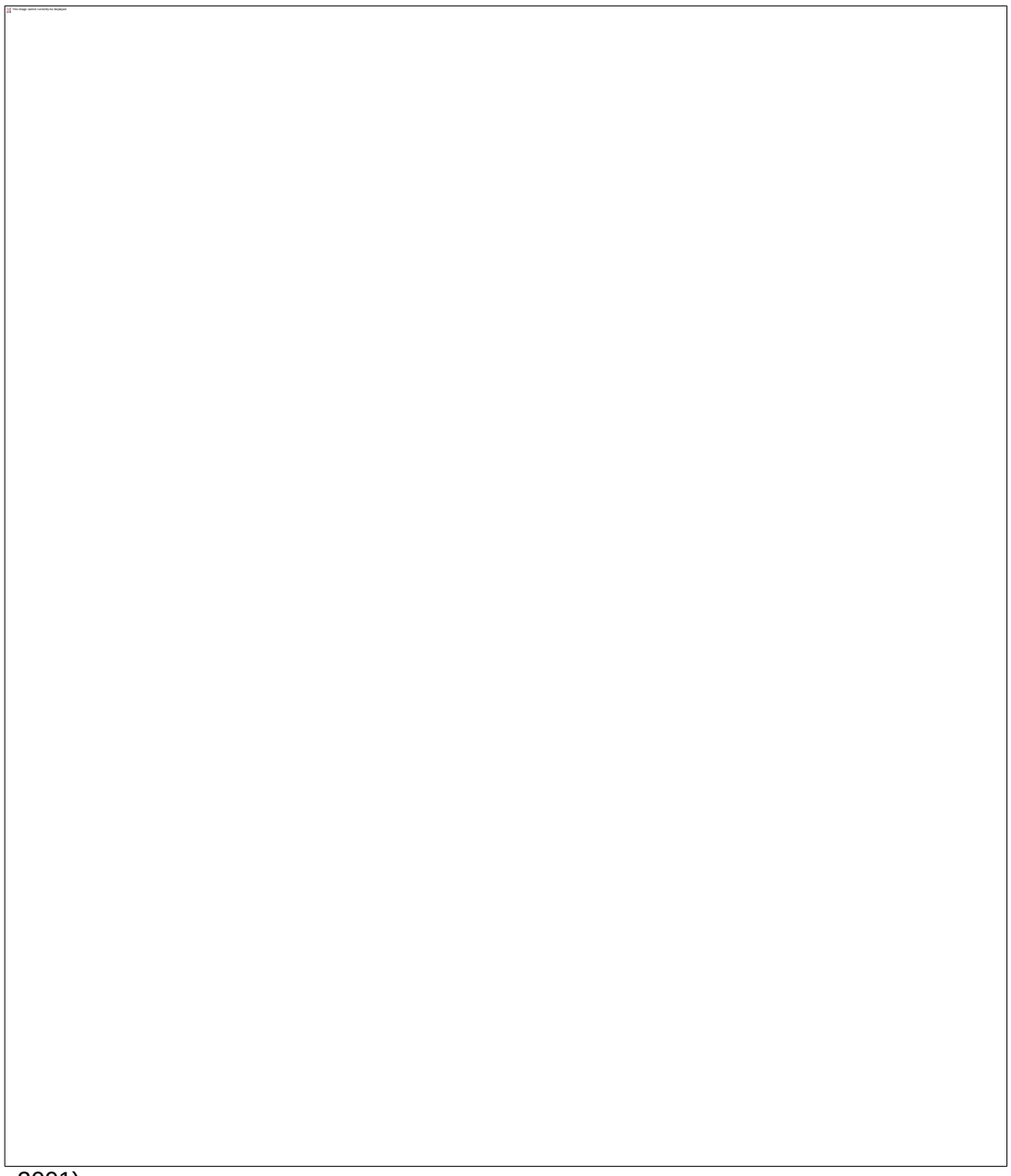

2001).

Figure 1-4 Southern Oklahoma Aulacogen evolution (Hoffman et al, 1974)

The Woodford Shale records a period of flooding during the late Paleozoic, when an epicontinental sea covered most of North America, with the deepest part being within the SOA (Roberts, 1992). Roberts (1992) suggests that the Woodford Shale was deposited over 10-15 million years, noting that cherts were deposited roughly 2.5 times faster than shales. Silica was deposited during short periods of high siliceous productivity as siliceous ooze (Watson, 2008). The Woodford Shale records a marine transgression from South to North (Over and Barrick, 1990). Paleogeographic maps of North America from Late Devonian and Early Mississippian are shown as figures 1-5 and 1-6. Over and Barrick (1990) suggest that the water depth was between 50 and 400 meters and the water column was stratified with anoxic bottom waters. Sediment sources for the Woodford Shale include the central Kansas uplift, the Chautauqua Arch, the St. Francois Mountains, and the Texas Arch (Johnson, 1989). Figure 1-7 shows the location of these sediment sources relative to the Oklahoma Basin at the time of Woodford deposition.

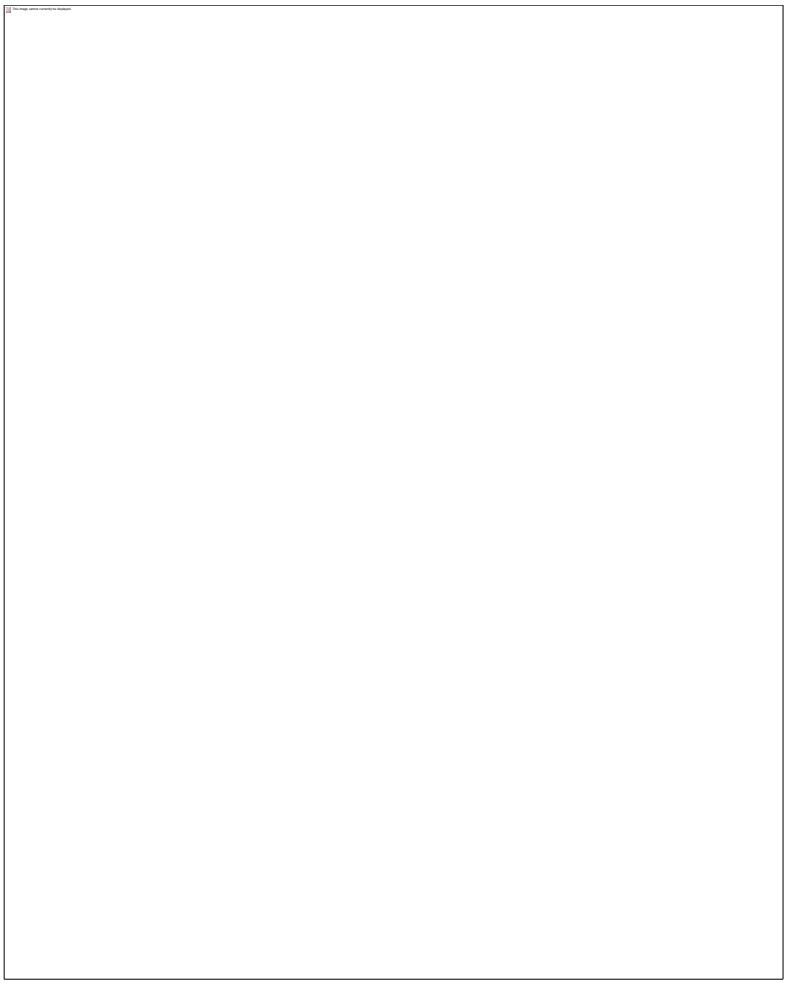

Figure 1-5 Late Devonian paleogeographic map (Blakey, 2013)

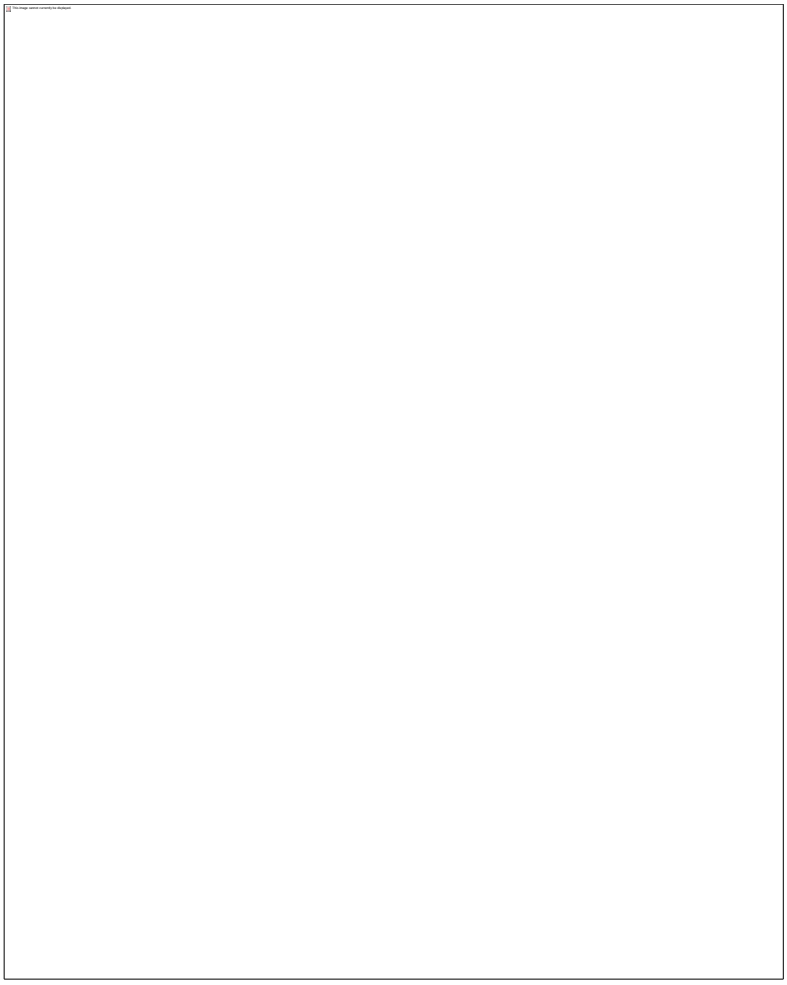

Figure 1-6 Early Mississippian paleogeographic map (Blakey, 2013)

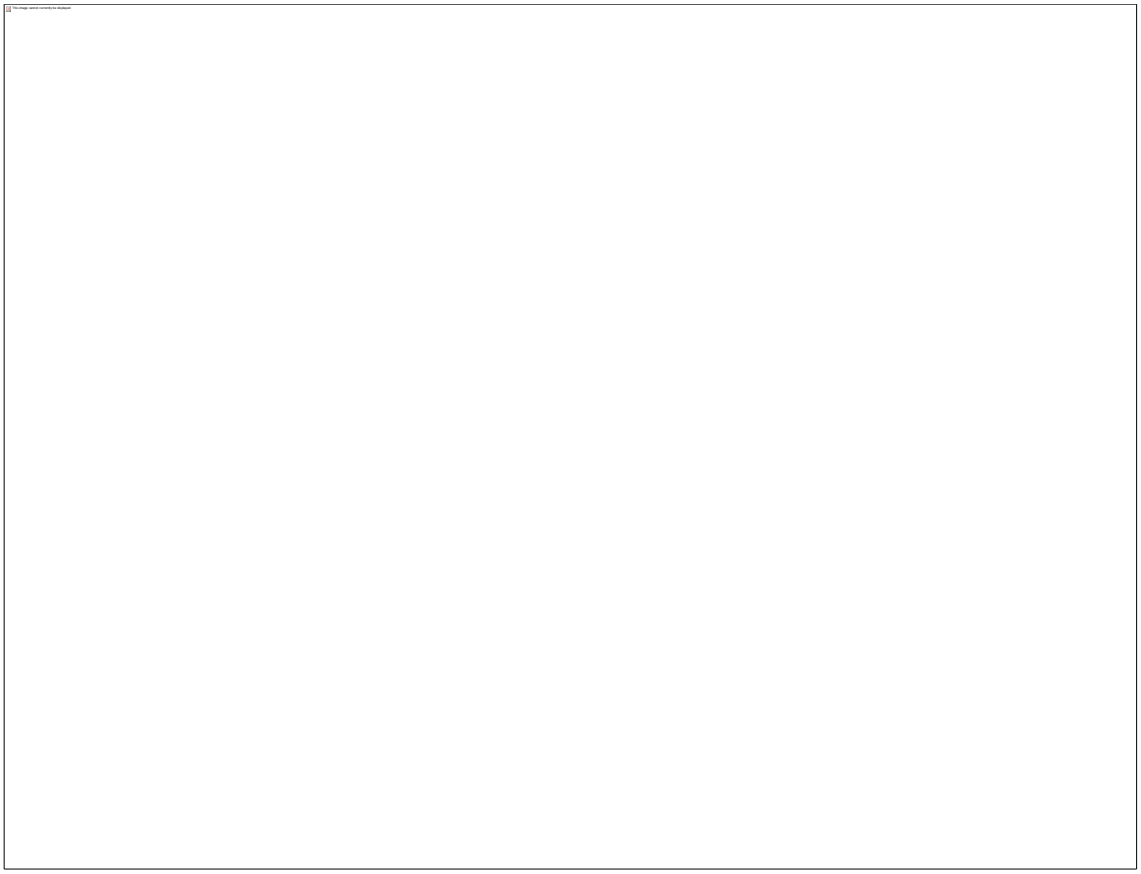

Figure 1-7 Map of south-central United States, showing features that existed during the early and middle Paleozoic (Johnson, 1989)

Deformation of the SOA began during the Morrowan. Crustal shortening was caused by the continental collision which resulted in the Ouachita orogenic belt (Fig. 1-4D). The Oklahoma Basin was divided into the Arkoma, Ardmore, and Anadarko proto-basins (Johnson, 1989). Intense folding and faulting occurred in the frontal Wichita fault zone and in the Anadarko Basin (Amsden, 1975).

Stratigraphy

The Woodford Shale unconformably overlies the Hunton Group in most of the Anadarko, Ardmore, and Arkoma Basins. Where the Hunton group is missing, the

Woodford Shale overlies the Sylvan Shale or, more rarely, the Viola Group (Watson, 2008). In the area of interest to the study, the Woodford Shale overlies the Hunton Group (Fig. 1-8). The Woodford Shale is overlain by Mississippi Limes (Fig. 1-9).

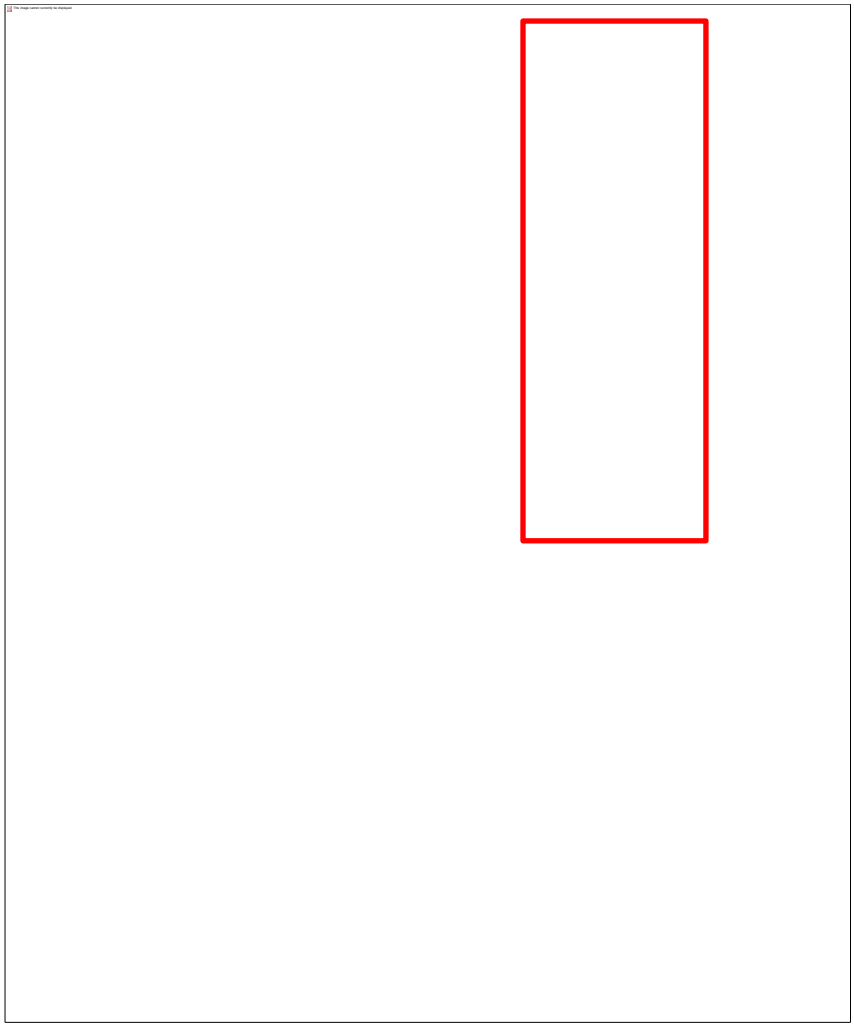

Figure 1-8 Paleogeographic map of the base of the Woodford Shale; study area is outlined in red (from Tarr, 1955)

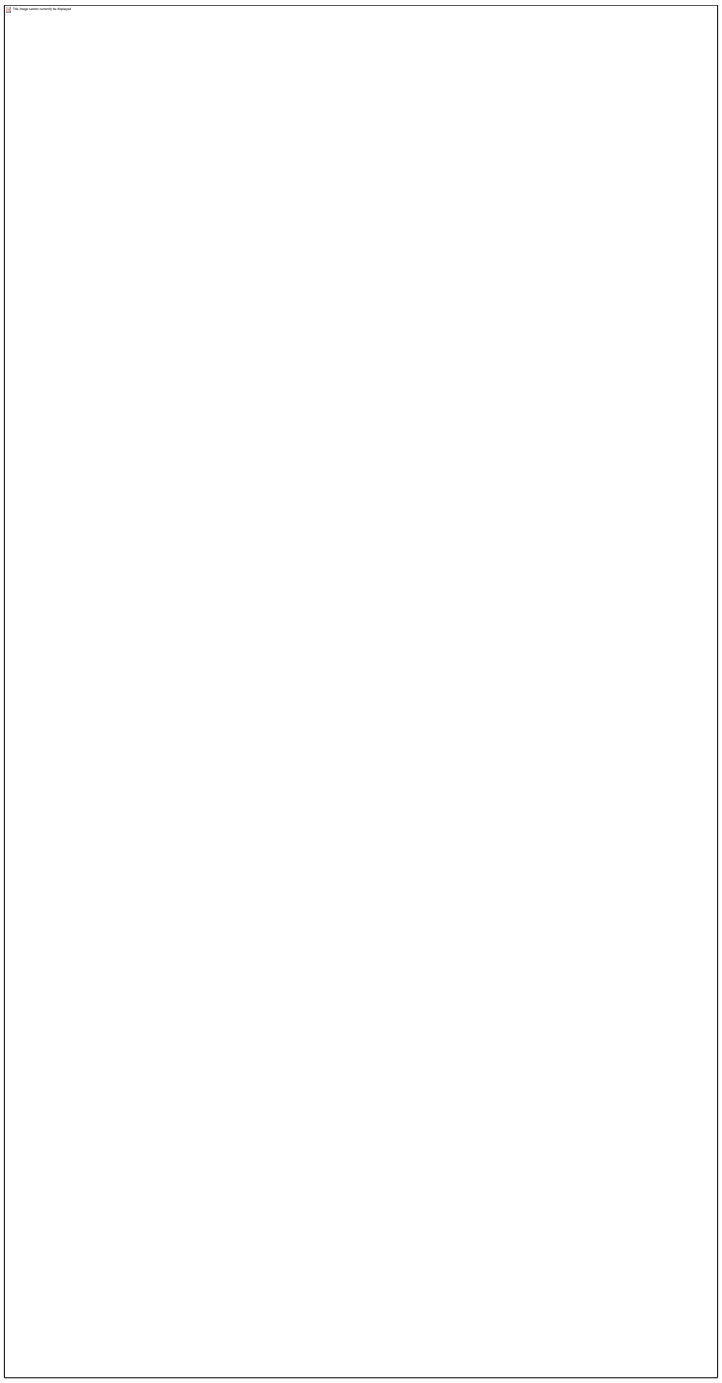

Figure 1-9 Generalized stratigraphic column of the Anadarko Basin (from Rose et al, 2004)

Chapter 2

Methods

Drill Core Information

Three drill cores of the Woodford Shale from three counties in central Oklahoma were studied (Table 2-1).

Table 2-1 Drill Core Information

Core Name	County	Location (Latitude/ Longitude)	API #	Number of Samples/ Length Analyzed
Shi Randall 4-29H	Grady	34.69646/ -97.74124	3505123539	1049 samples 387 feet
Ridenour 1-20H	Canadian	35.50719/ -98.18344	3501724113	657 samples 173 feet
Teague 1-14H	Kingfisher	35.63836/ -98.10087	3507324724	582 samples 204 feet

Energy dispersive X-ray fluorescence (ED-XRF) analyses were performed at 3-4 inch intervals for each core. Samples were labeled and photographed before being analyzed. A depth model was constructed for each core and correlated with the ED-XRF data. For the Teague 1-14H core, only the dark shale zone was analyzed for trace elements.

Energy Dispersive X-Ray Fluorescence (ED-XRF)

Elemental analyses were performed using a Bruker Tracer III/IV energy dispersive X-ray fluorescence analyzer (Fig. 2-1). The ED-XRF instrument was kept stationary during analysis and the flat surface of the slabbed cores was placed on the detector window of the instrument. A flat surface is required for ED-XRF analysis to minimize loss of sensitivity of the instrument. Each sample was analyzed twice, once for major elements and once for trace elements. Major elements detected are (reported in

weight percent) magnesium (Mg), aluminum (Al), silicon (Si), phosphorus (P), potassium (K), calcium (Ca), titanium (Ti), Manganese (Mn), and iron (Fe); vanadium (V) and chromium (Cr) are also detected and reported in parts-per-million (ppm). Major element analysis was performed using a low voltage setting with a vacuum pump for a count time of 60 seconds. Trace elements detected include cobalt (Co), nickel (Ni), copper (Cu), zinc (Zn), thorium (Th), rubidium (Rb), uranium (U), strontium (Sr), zirconium (Zr), and molybdenum (Mo). Trace element analysis was performed using a high voltage setting with a filter for a count time of 60 seconds. Major and trace element calibrations were performed by Rowe et al. (2012) using 90 references of known composition: 5 international shale standards, 7 from the Ohio Shale, 20 from the Smithwick Formation, 27 from the Woodford Shale, 15 from the Eagleford Formation, and 16 from the Barnett Shale. Each of these 90 references was analyzed for 180 seconds 3 times, for a total of 270 analyses. The 270 raw XRF spectra were loaded into Bruker's CalProcess software to yield calibrations for both low and high energy settings. A standard was analyzed for 180 seconds at the beginning and end of each sampling day to ensure proper instrument calibration.

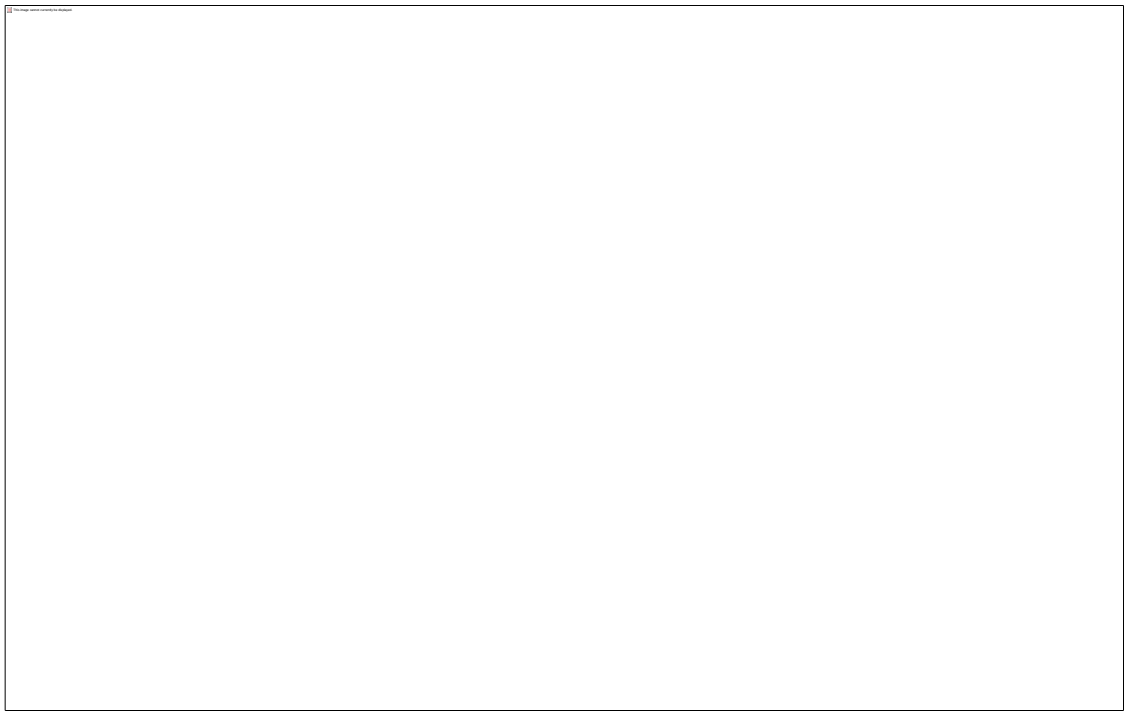

Figure 2-1 The Bruker III/IV ED-XRF Instrument. (A) Operating instrument set-up; (B) Operating instrument set-up including the vacuum pump, which is used in low energy data collection (major elements); (C) Close-up of the nose of the instrument showing where filters used for high-energy data collection (trace elements) are inserted; (D) Top view of the instrument showing the beam window; (E) the Si-PIN detector.

Chapter 3

Methods

Shi Randall 4-29H

Elemental concentration, in percent weight, of calcium (Ca), aluminum (Al), and silica (Si), as well as the ratio of silica to aluminum (Si/Al) by depth is shown in figure 3-1 for the Shi Randall 4-29H core. Five zonations were made based on variations in Ca, Al, and Si. Zone A (shown by red circles) is characterized by extreme Ca pulses, overall increasing Al concentration, and variably high Si. Zone B (shown by black squares) is characterized by fewer calcium pulses than zone A, slightly higher Al concentration than zone A, and high, less variable Si concentration. Zone C (denoted by green triangles) is characterized by very high Si concentration, highly variable Al concentration, and few Ca pulses. Zone D (denoted by gray circles) is characterized by no Ca pulses, very high Al concentration, and lower Si concentration (~28%). Zone E (shown by blue squares) is characterized by decreasing Al concentration down-core, and high Si concentration. Si/Al shows high variability in all zones, except zone D. Variability of Si/Al also has slightly less variability in zone B than in other zones.

Figure 3-2 shows elemental concentrations, in percent weight, of titanium (Ti), potassium (K), magnesium (Mg), iron (Fe), and sulfur (S). Co-variation is observed between Ti and K, as well as Fe and S. Differences in the concentration of these elements appear to generally coincide with the zonations made based on Si, Ca, and Al.

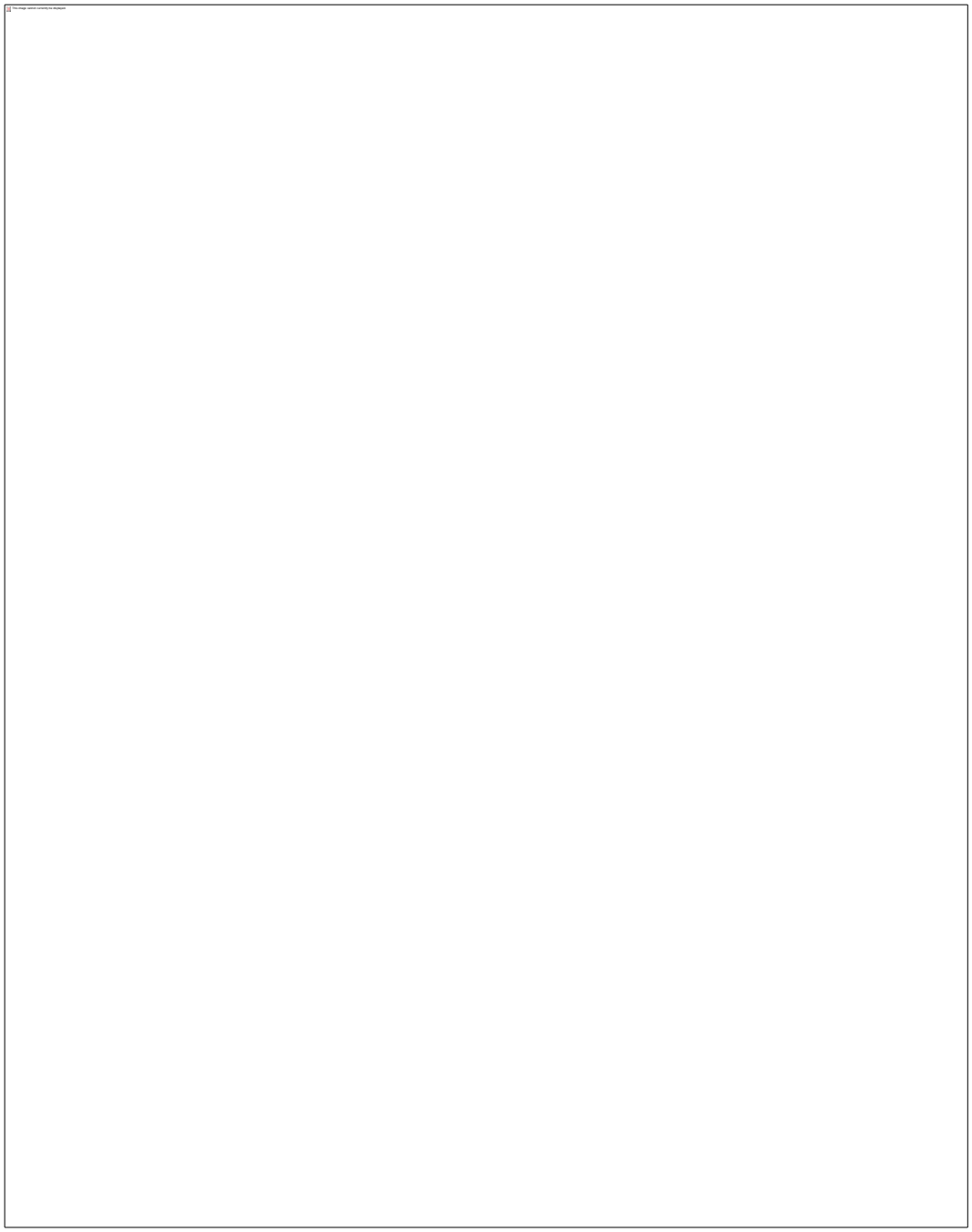

Figure 3-1 Down-core plot of %Ca, %Al, %Si, and Si/Al for the Shi Randall 4-29H core

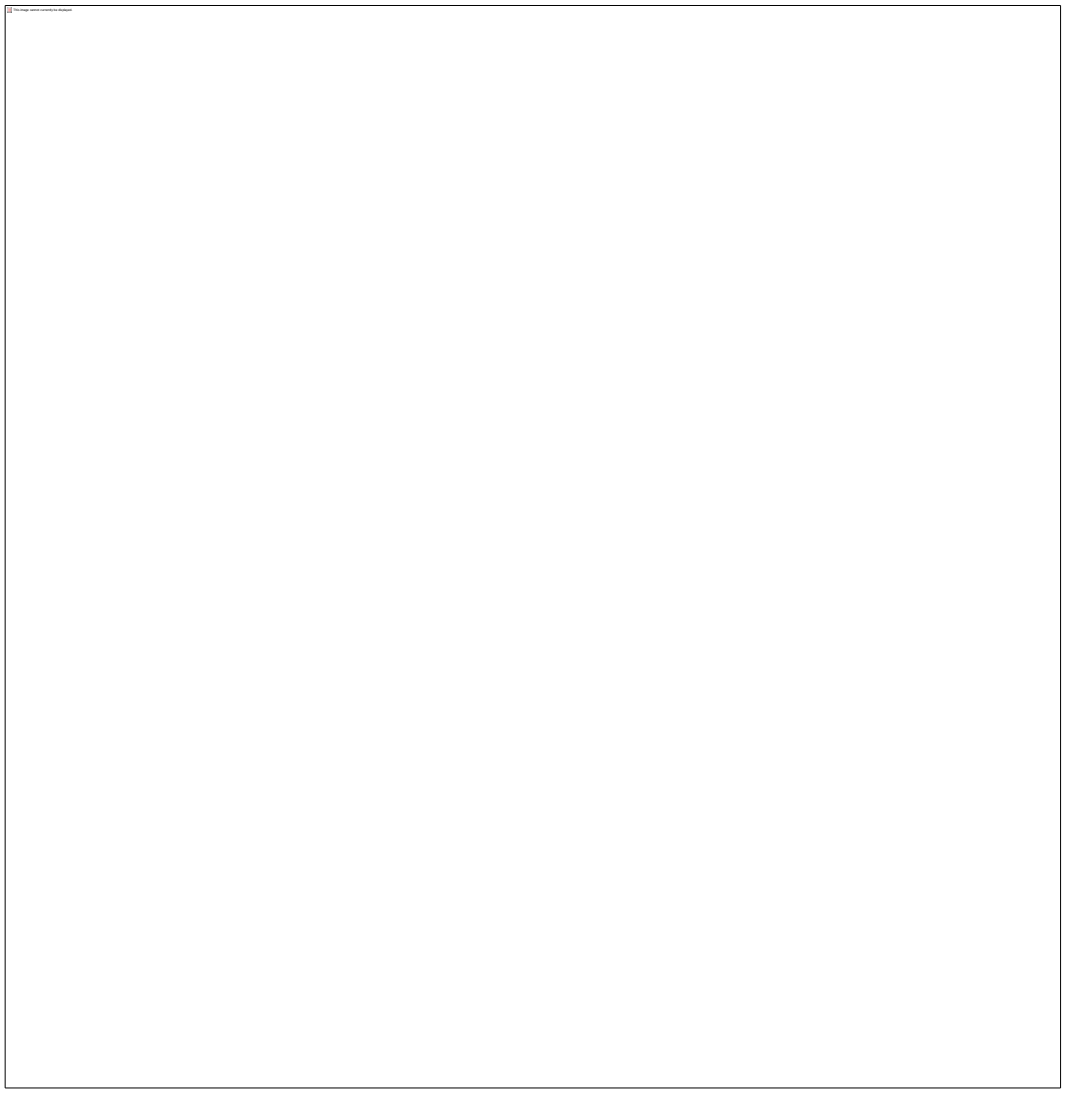

Figure 3-2 Down-core plot of %Ti, %K, %Mg, %Fe, and %S for the Shi Randall 4-29H core

A ternary diagram; with clay, calcite, and quartz end members; is shown in figure 3-3. Percent weight values of Si, Al, and Ca were converted to their oxide forms: SiO_2, Al_2O_3, and CaO; the values were then normalized. The composition of an average

gray shale (Wedepohl, 1971) is indicated by a red star for reference. Most samples from the Shi Randall 4-29H core fall toward to quartz end member, with few samples falling toward the calcite end member. The samples that fall towards the CaO end member correspond to the Ca pulses seen in the down core plot (fig. 3-1).

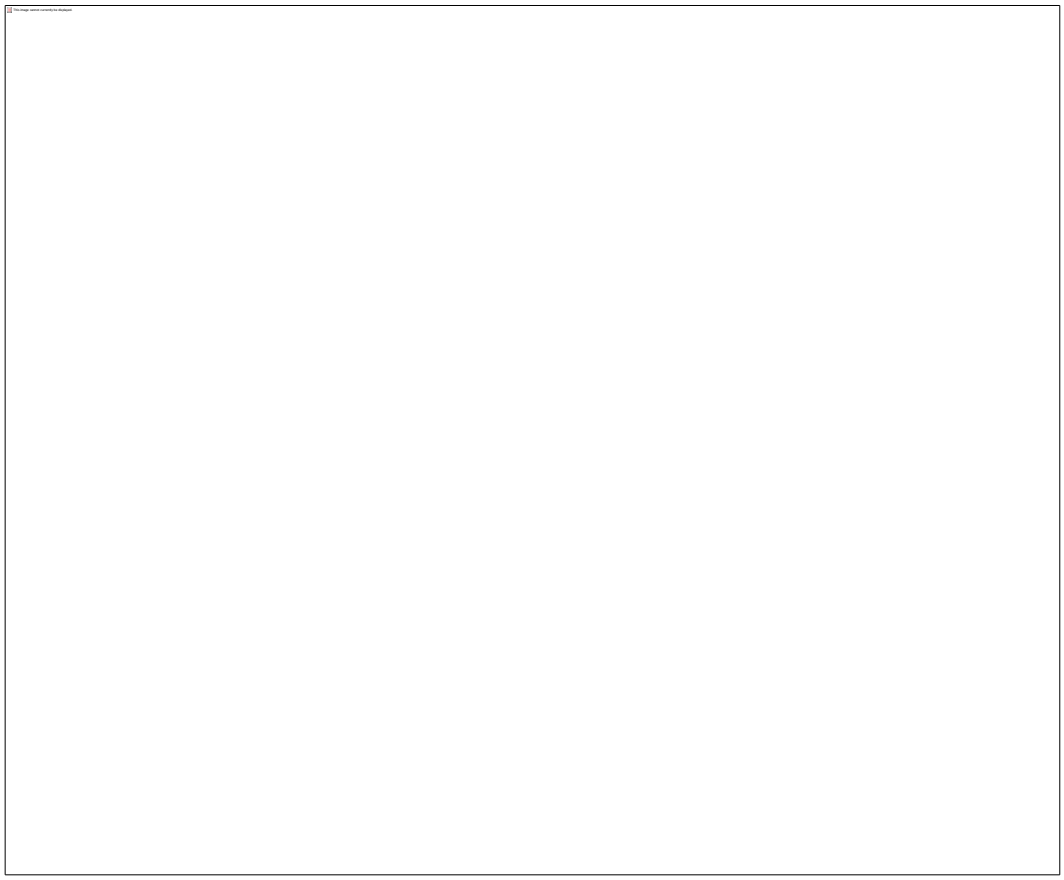

Figure 3-3 Ternary diagram for the Shi Randall 4-29H core; calcium oxide (CaO), alumina (Al_2O_3), and silica (SiO_2)

Figure 3-4 shows various major elements plotted against Al to show the relationship between these elements and the clay fraction of the sample. Si *versus* Al (fig. 3-4A) shows a negative linear trend with several samples plotting below the trend line. Most samples plotting below the trend line are from the red and black zones. Ca *versus* Al (fig. 3-4B) shows neither a strong positive nor negative correlation. The samples plotting above the majority correspond to the Ca pulses observed in the down-core plot (fig. 3-1). These samples show a weak negative correlation between Ca and Al. K *versus* Al (fig. 3-4C) shows a strong positive linear correlation. P *versus* Al does not show either a positive or negative correlation. Ti *versus* Al (fig. 3-4E) shows a strong positive linear correlation. Fe *versus* Al shows a weak positive correlation, overall. Samples from the red and black zones appear to show the weakest correlation.

Figure 3-4 Major element cross-plots for the Shi Randall 4-29H core: (A) %Si versus %Al; (B) %Ca versus %Al; (C) %K versus %Al; (D) %P versus %Al; (E) %Ti versus %Al; (F) %Fe versus %Al

1971; Calvert and Pederson, 1993). Enrichment factors are calculated using the following equation:

$$EF = (\text{element in ppm/Al in ppm})_{sample} / (\text{element in ppm/Al in ppm})_{average\ gray\ shale}$$

The elemental concentration for trace elements and aluminum for an average gray shale is taken from Wedepohl (1971). If EF is greater than 1 for any given element, that sample is said to be enriched in that element. If EF is less than 1, the sample is depleted in that element, compared to an average gray shale.

Nearly all samples in the Shi Randall 4-29H core are enriched in molybdenum, chromium, uranium, nickel, zinc, and copper (fig. 3-6). The black zone and the gray zone show the least amount of enrichment, with most samples in the gray zone being depleted in Mo, Zn, Ni, and Cu. It should be noted that several samples in the uppermost portion of the red zone are not shown on the graph for Zn and Cu due to very high enrichment factors in the samples. They were excluded in order to provide better resolution of the remainder of the samples.

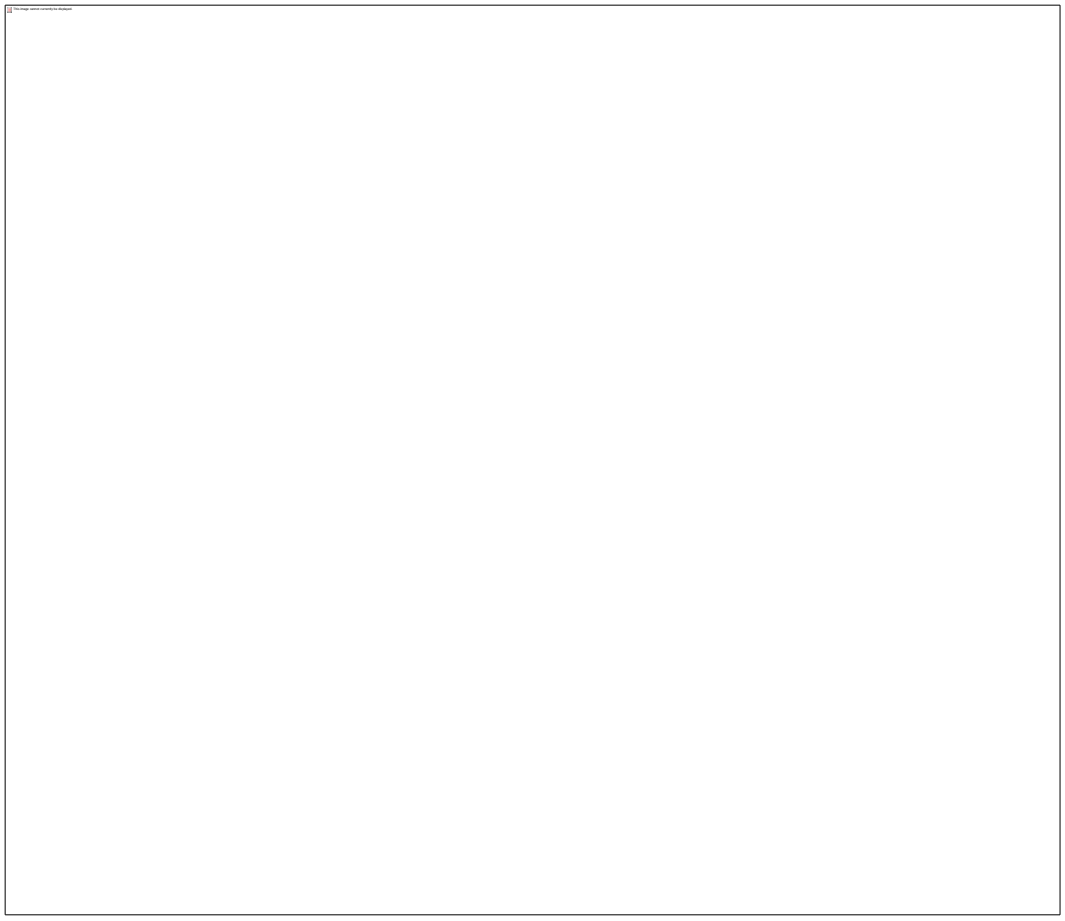

Figure 3-6 Down-core plot of the enrichment factors (EF) of Mo, Cr, U, Ni, Zn, and Cu for the Shi Randall 4-29H core

Figure 3-7 shows the enrichment factor of manganese plotted by depth, as well as trace element ratios: Ni/Co, V/Cr, and V/(V+Ni). These ratios were chosen because they have been found to be indicative of paleoredox conditions (Hatch and Leventhal, 1992; Jones and Manning, 1994; Rimmer, 2003). The enrichment factor of manganese is shown because it can also be used as an indicator of paleoredox conditions and longevity (Calvert and Pederson, 1993). Table 1 shows the suggested

values indicative of different paleoredox conditions for each EF or ratio, along with the color coding.

Table 3-1. Paleoredox condition indicators (from Hatch and Leventhal, 1992; Calvert and Pederson, 1993; Jones and Manning, 1994; Rimmer, 2003)

Paleoredox Condition	EF Mn	Ni/Co	V/Cr	V/(V+Ni)	Color
Oxic	>1	<5	<2	<0.46	Blue
Dysoxic	-	5-7	2-4.25	0.46-0.60	Green
Suboxic to anoxic	<1	>7	>4.25	0.54-0.82	Red
Euxinic	-	-	-	<0.84	Gray

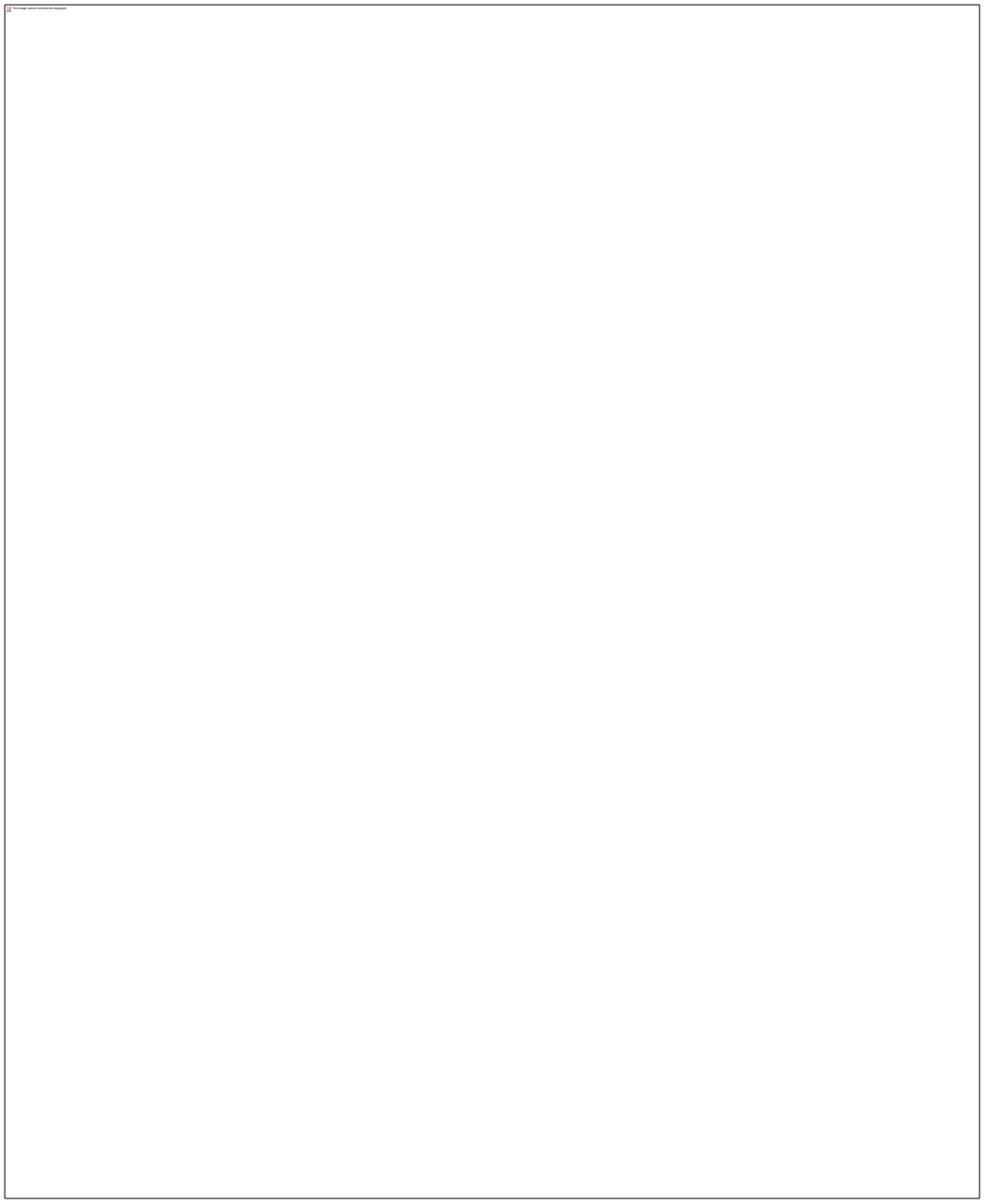

Figure 3-7 Down-core plot of EF Mn, Ni/Co, V/Cr, and V/(V+Ni) for the Shi Randall 4-29H core

Ridenour 1-20H

Elemental concentration, in percent weight, of calcium (Ca), aluminum (Al), and silica (Si), as well as the ratio of silica to aluminum (Si/Al) by depth is shown in figure 3-8 for the Ridenour 1-20H core. Three zonations were made based on variations in Ca, Al, and Si. Zone A (shown by red circles) is characterized by extreme Ca pulses, variable Al concentration, and variably high Si. Zone B (shown by black squares) is characterized by less variation in Al concentration than zone A, and high, less variable Si concentration. Zone C (denoted by green triangles) is characterized by slightly lower Si concentration than in zones A and B and generally high Al concentration. Si/Al shows low variability in zones B and C, with a few pulses of silica enrichment over aluminum.

Figure 3-8 Down-core plot of %Ca, %Al, %Si, and Si/Al for the Ridenour 1-20H core

Figure 3-9 shows elemental concentrations, in percent weight, of titanium (Ti), potassium (K), magnesium (Mg), iron (Fe), and sulfur (S). Co-variation is observed

between Ti and K, as well as Fe and S. General differences in the concentration of these elements appear to generally coincide with the zonations made based on Si, Ca, and Al (fig. 3-8).

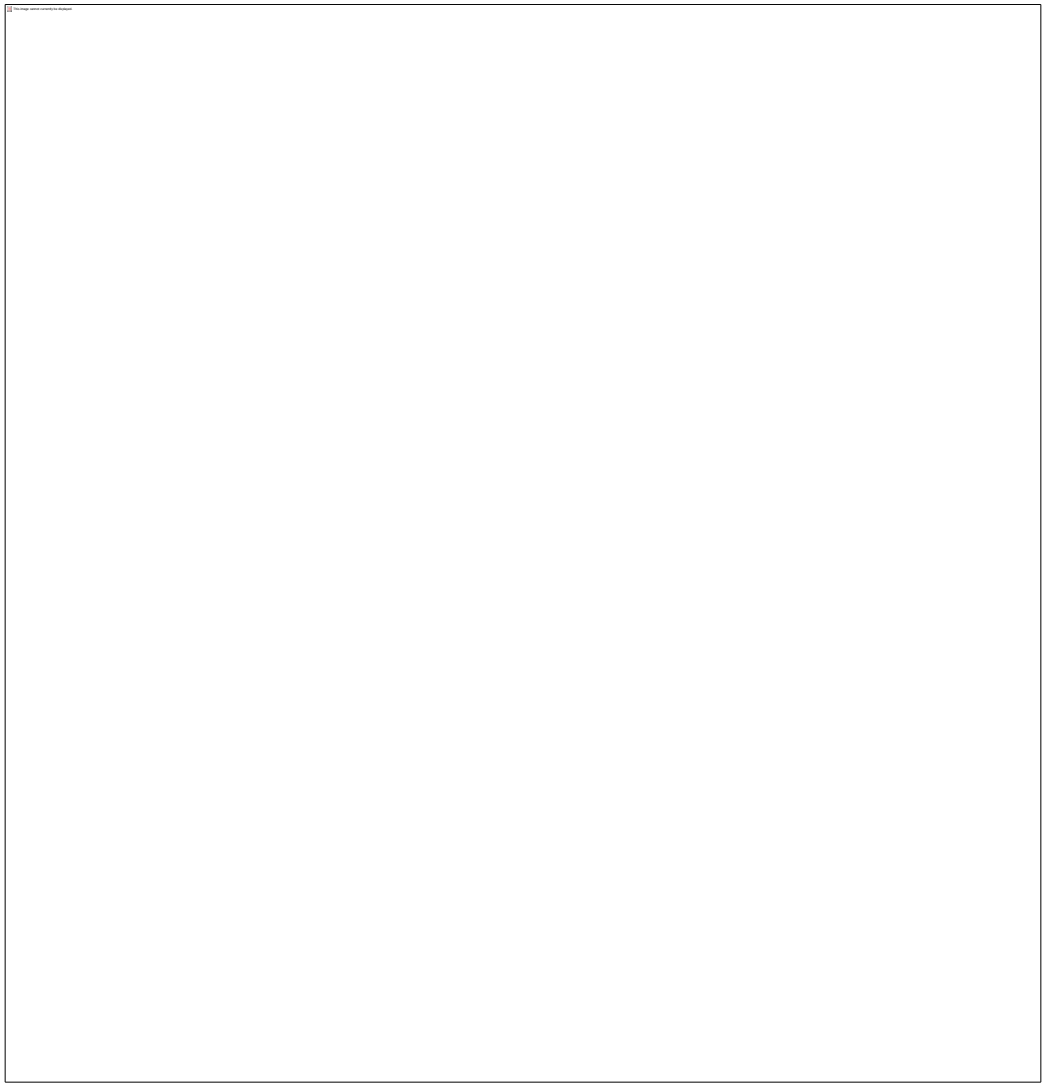

Figure 3-9 Down-core plot of %Ti, %K, %Mg, %Fe, and %S for the Ridenour 1-20H core

A ternary diagram; with clay, calcite, and quartz end members; for the Ridenour 1-20H core is shown in figure 3-10. Values were calculated and normalized as

previously mentioned. The composition of an average gray shale (Wedepohl, 1971) is indicated by a red star for reference. Most samples from the Ridenour 1-20H core fall toward to quartz end member, with few samples falling toward the calcite end member. The samples that fall towards the CaO end member correspond to the Ca pulses seen in the down core plot (fig. 3-8).

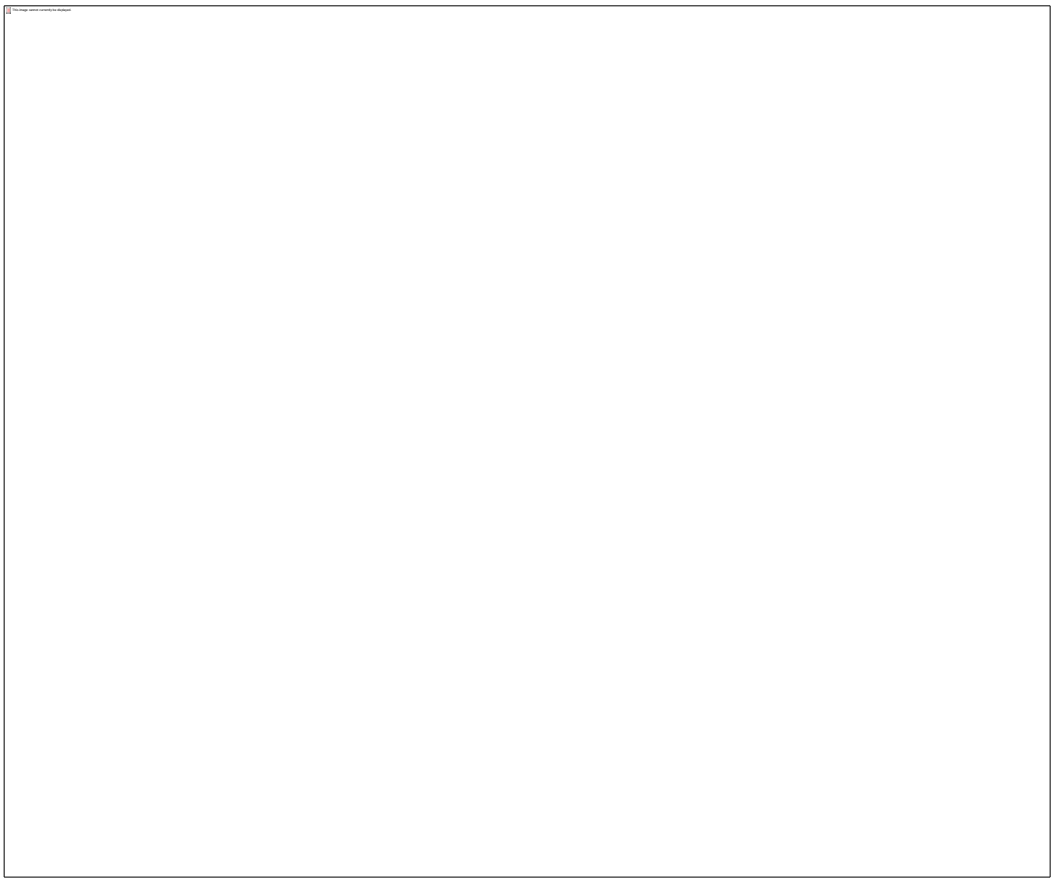

Figure 3-10 Ternary diagram for the Ridenour 1-20H core; calcium oxide (CaO), alumina (Al2O3), and silica (SiO2)

Figure 3-11 shows various major elements plotted against Al to show the relationship between these elements and the clay fraction of the sample. Si *versus* Al (fig. 3-11A) shows a negative linear trend with a few samples plotting below the trend line.

Samples plotting below the general trend line correspond to samples with high Ca concentration. Ca *versus* Al (fig. 3-11B) shows neither a strong positive nor negative correlation. The samples plotting above the majority correspond to the Ca pulses observed in the down-core plot (fig. 3-8). K *versus* Al (fig. 3-11C) shows a strong positive linear correlation. P *versus* Al (fig. 3-11D) does not show either a positive or negative correlation. Ti *versus* Al (fig. 3-11E) shows a strong positive linear correlation. Fe *versus* Al (fig. 3-11F) shows a weak positive linear correlation. Several samples plot above the general correlation line.

Figure 3-11 Major element cross-plots for the Shi Randall 4-29H core: (A) %Si *versus* %Al; (B) %Ca *versus* %Al; (C) %K *versus* %Al; (D) %P *versus* %Al; (E) %Ti *versus* %Al; (F) %Fe *versus* %Al

Figure 3-12 shows a cross-plot of %Fe *versus* %S. Overlain are four trend lines representing the degree of pyritization (DOP), as previously discussed (Levanthal, 1979; Raiswell et al, 1988; Robinson, 2012). There is a general trend observed along the pyrite line, but significant scatter is also observed.

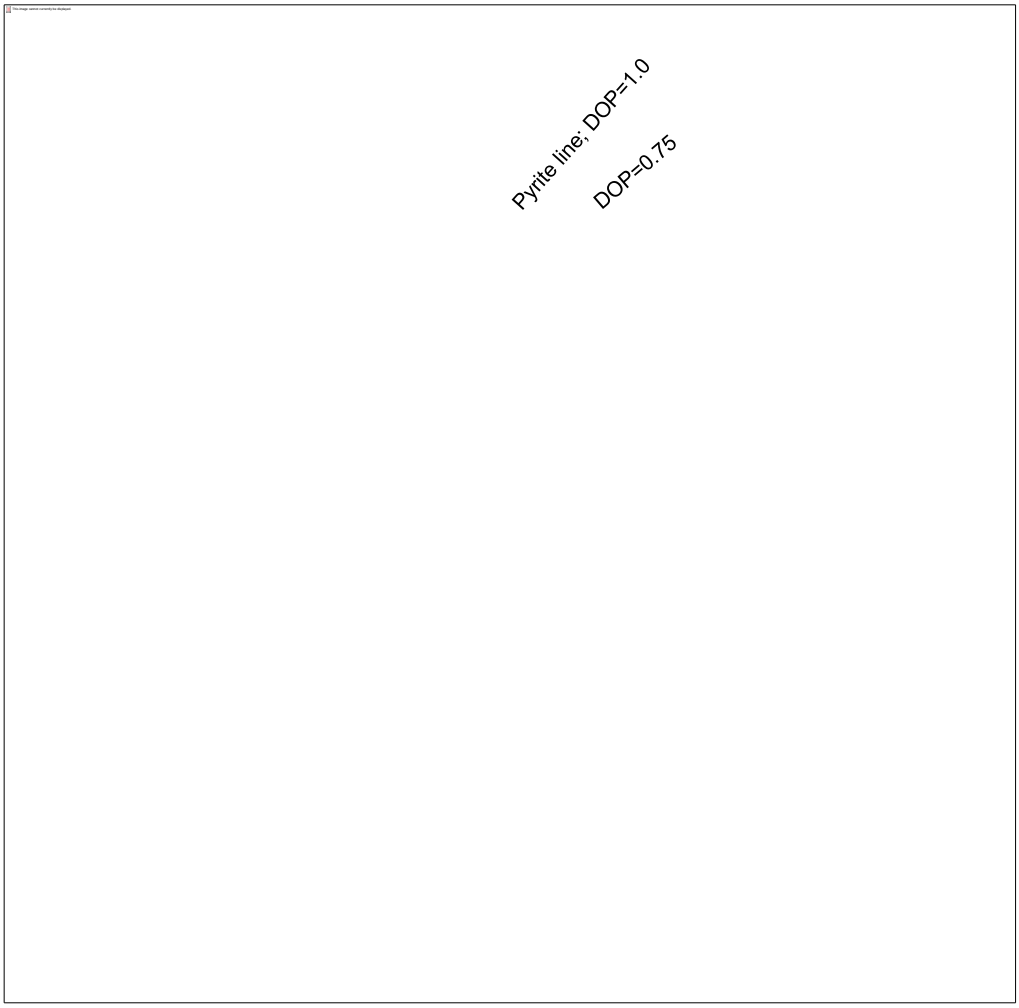

Figure 3-12 Cross-plot of %Fe *versus* %S for the Ridenour 1-20H core

Figure 3-13 shows various trace element enrichment factors plotted by depth for the Ridenour 1-20H core. Enrichment factors are used here to determine if a

sample is enriched in a given trace element relative to an average gray shale, as previously discussed (Wedepohl, 1971; Calvert and Pederson, 1993).

Most samples in the Ridenour 1-20H core are somewhat enriched in molybdenum, chromium, uranium, nickel, zinc, and copper (fig. 3-13). However, the black and green zones also record periods of depletion of these trace elements, most markedly, chromium.

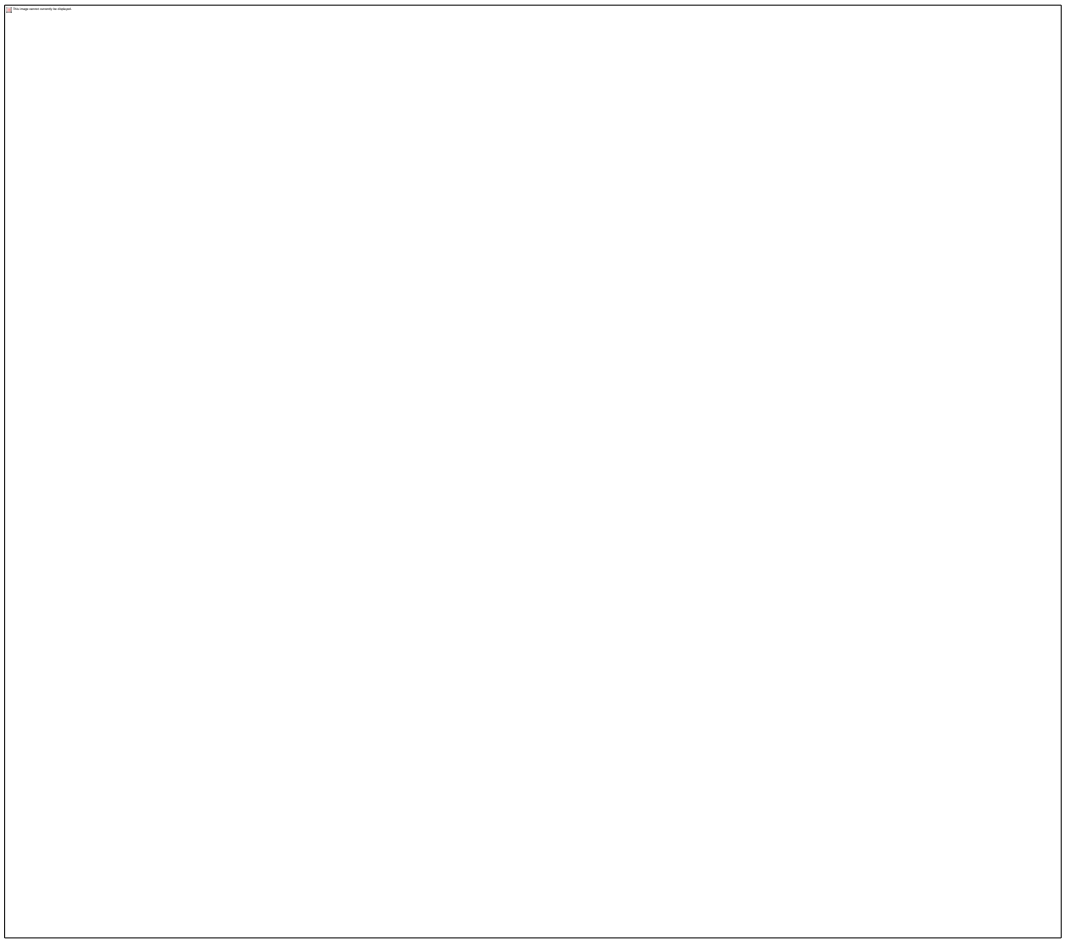

Figure 3-13 Down-core plot of the enrichment factors (EF) of Mo, Cr, U, Ni, Zn, and Cu for the Shi Randall 4-29H core.

Figure 3-14 shows the enrichment factor of manganese plotted by depth, as well as trace element ratios: Ni/Co, V/Cr, and V/(V+Ni) for the Ridenour 1-20H core. These ratios were chosen because they have been found to be indicative of paleoredox conditions, as previously discussed (Hatch and Leventhal, 1992; Jones and Manning, 1994; Rimmer, 2003). The enrichment factor of manganese is shown because it can also be used as an indicator of paleoredox conditions and longevity (Calvert and Pederson, 1993). It should be noted that some samples with ratios of very high magnitude were excluded in order to provide better resolution for the general population of samples. The majority of the samples from the Ridenour 1-20H core do not show Mn enrichment. The highest overall magnitudes for each of the trace element ratios are observed in the red and green zones.

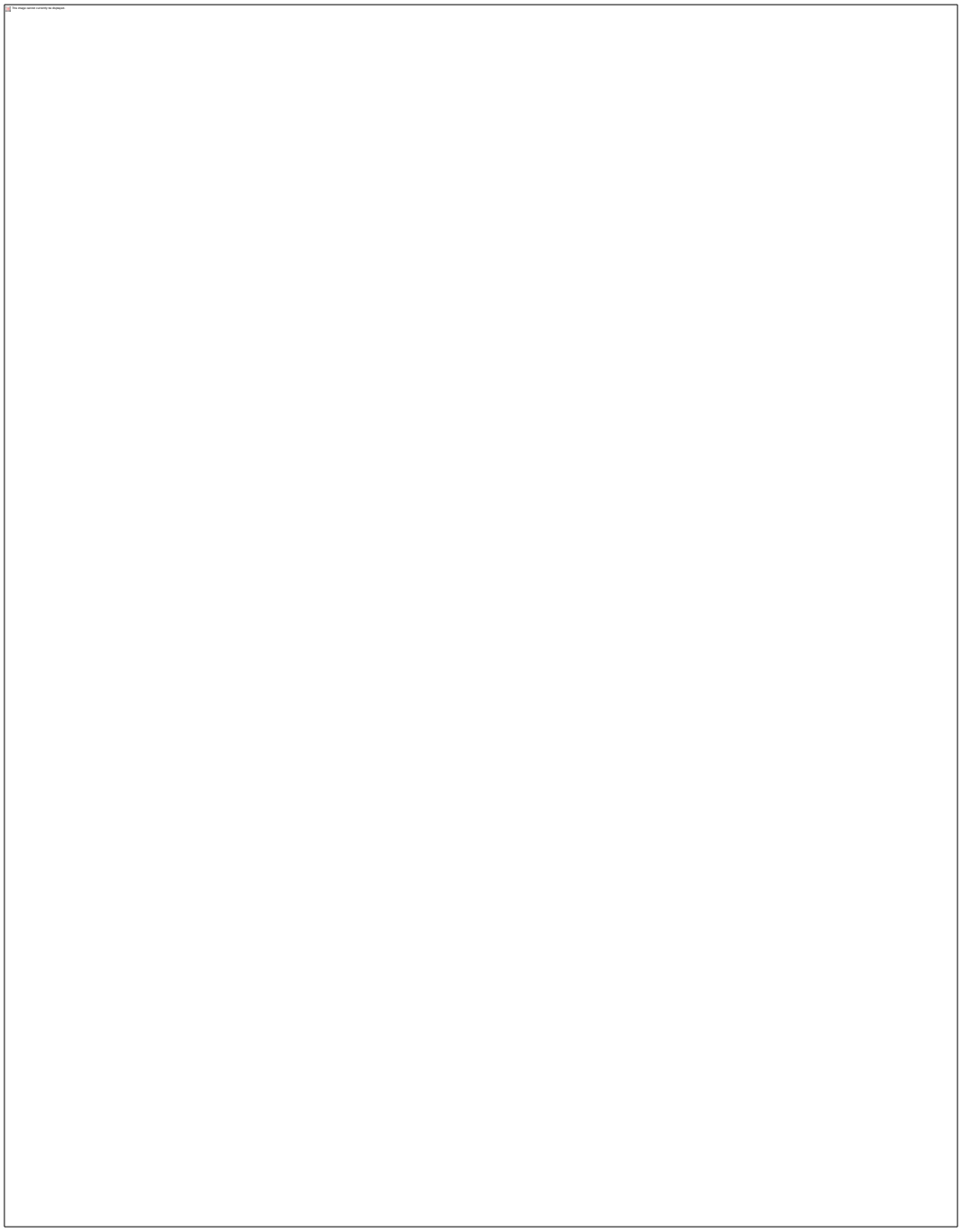

Figure 3-14 Down-core plot of EF Mn, Ni/Co, V/Cr, and V/(V+Ni) for the Ridenour 1-20H core

Teague 1-14H

Elemental concentration, in percent weight, of calcium (Ca), aluminum (Al), and silica (Si), as well as the ratio of silica to aluminum (Si/Al) by depth is shown in figure 3-15 for the Teague 1-14H core. Four zonations were made based on variations in Ca, Al, and Si. Zone A (shown by red circles) is characterized by high Ca concentration with variability, low Al concentration, and variable Si concentration. Zone B (shown by black squares) is characterized by generally high Ca concentration with lower frequency variability than zone A, slightly higher Al concentration than zone A, and high Si concentration with lower frequency variability than in zone A. Zone C (denoted by green triangles) is characterized by low Ca concentration, higher Al concentration than in zone A or B with significant variability, and very high Si concentration. Zone D (shown as gray circles) is characterized by low Ca concentration, overall high Al concentration, and high Si concentration (although slightly lower than in zone C). Si/Al shows low variability in zones B and D, with a few pulses of silica enrichment over aluminum in zone B. More variability in Si/Al is observed in zones A and C, with the highest Si to Al ratios being observed in the bottom of zone C.

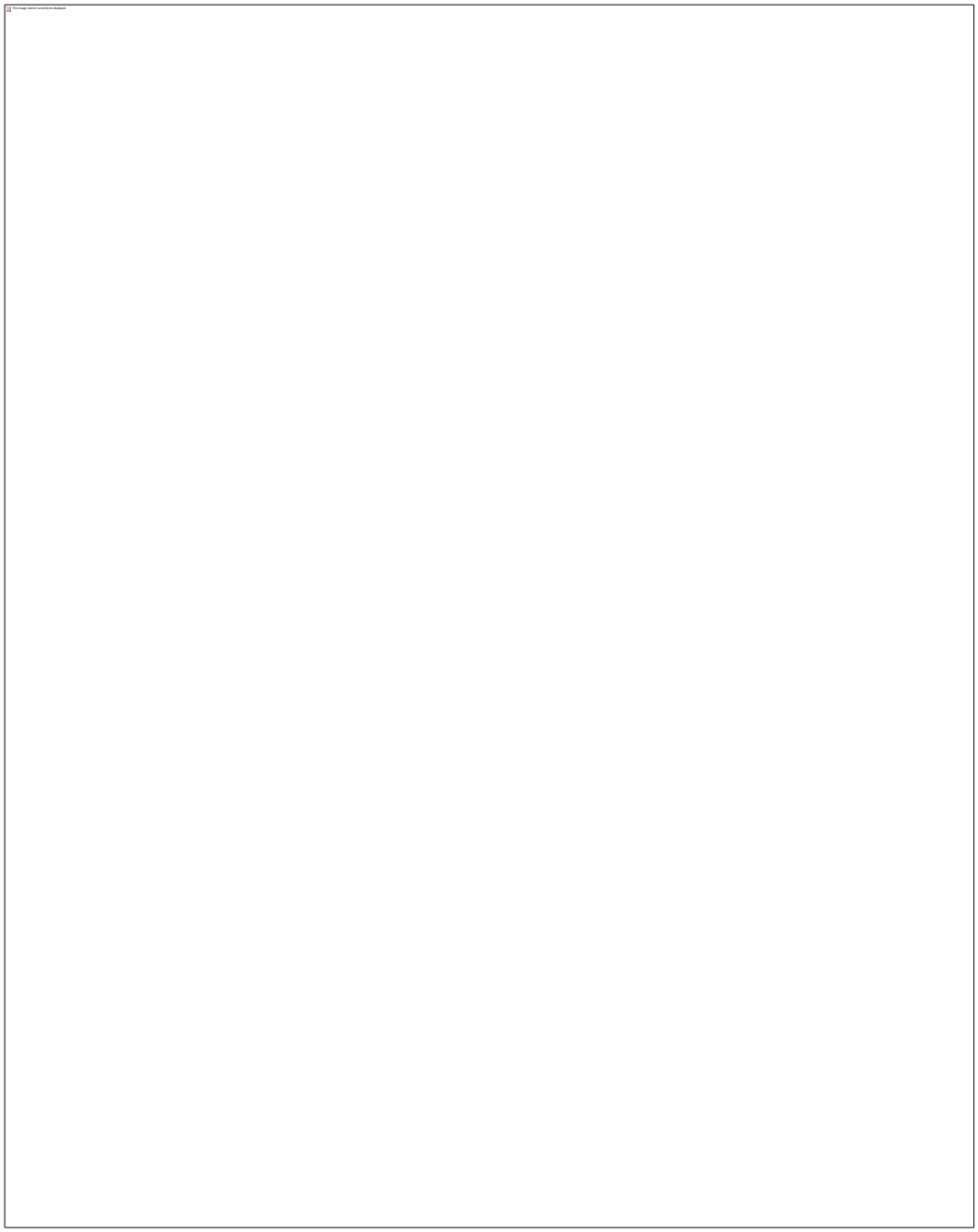

Figure 3-15 Down-core plot of %Ca, %Al, %Si, and Si/Al for the Teague 1-14H core

Figure 3-16 shows elemental concentrations, in percent weight, of titanium (Ti), potassium (K), magnesium (Mg), iron (Fe), and sulfur (S). Strong co-variation is observed between Ti and K, as well as slightly weaker co-variation between Fe and S. General differences in the concentration of these elements appear to generally coincide with the zonations made based on Si, Ca, and Al (fig. 3-15).

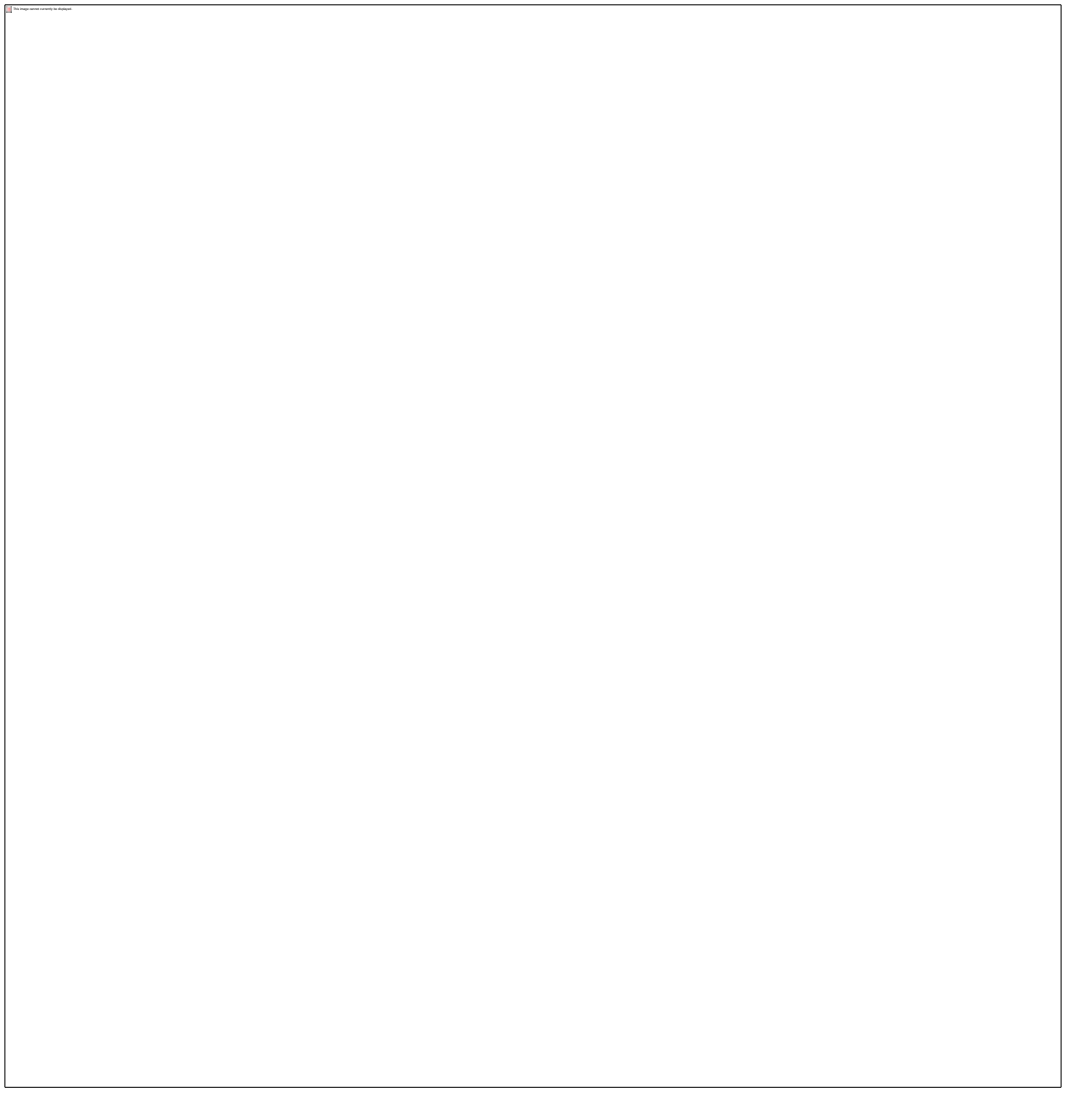

Figure 3-9 Down-core plot of %Ti, %K, %Mg, %Fe, and %S for the Ridenour 1-20H core

A ternary diagram; with clay, calcite, and quartz end members; for the Teague 1-14H core is shown in figure 3-17. Values were calculated and normalized as previously mentioned. The composition of an average gray shale (Wedepohl, 1971) is indicated by a red star for reference. Most samples from zones C and D (green and gray) of the Teague 1-14H core fall toward to quartz end member, with samples from zones A and B (red and black) falling toward the calcite end member.

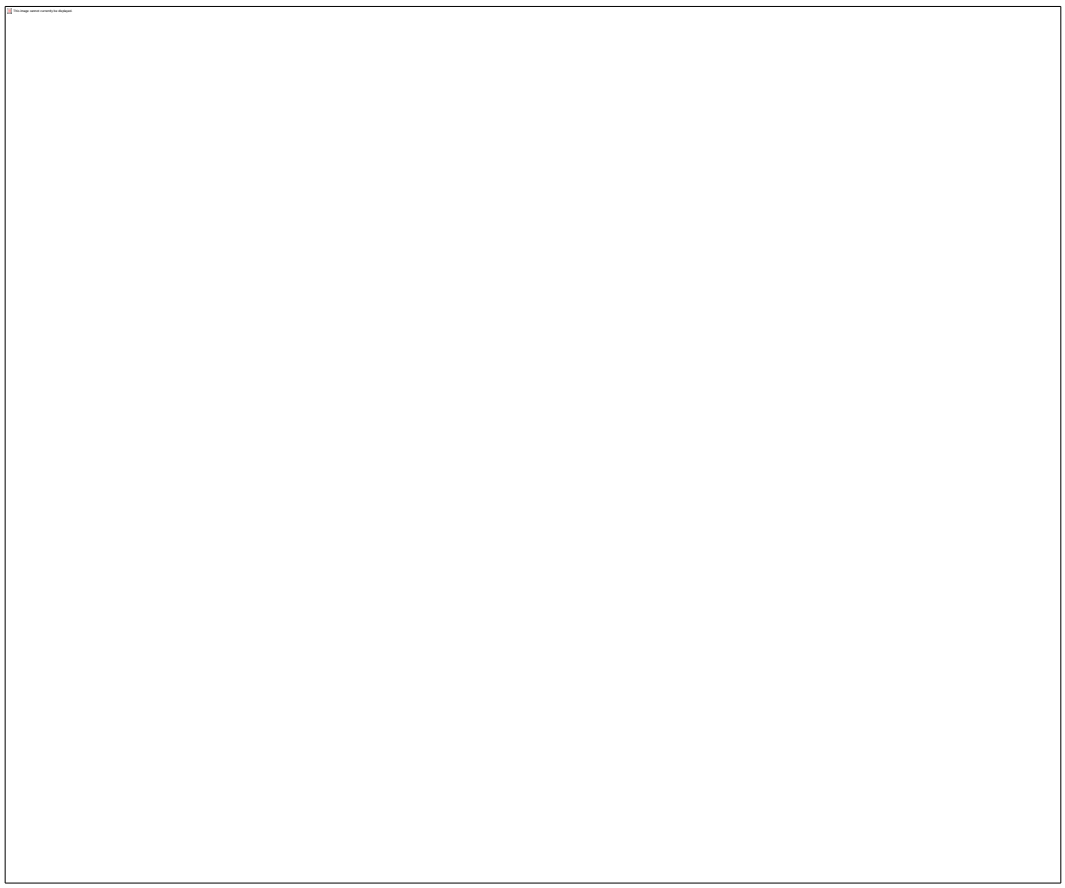

Figure 3-17 Ternary diagram for the Teague 1-14H core; calcium oxide (CaO), alumina (Al_2O_3), and silica (SiO_2)

Figure 3-18 shows various major elements plotted against Al to show the relationship between these elements and the clay fraction of the sample. Si *versus* Al (fig. 3-18A) shows a negative linear trend for samples from zones C and D (green and gray). Samples from zones A and B (red and black) are plotted below this negative trend line in an almost vertical trend. Ca *versus* Al (fig. 3-18B) shows a steep negative linear correlation of samples from zones A and B, and no identifiable correlation between those from zones C and D. K *versus* Al (fig. 3-18C) shows a strong positive linear correlation for samples from all four zones. P *versus* Al (fig. 3-18D) does not show either a positive or negative correlation. Ti *versus* Al (fig. 3-18E) shows a strong positive linear correlation for samples from all four zones. Fe *versus* Al (fig. 3-18F) shows a positive linear correlation for samples from all four zones, with zone D (gray) showing the weakest correlation. Several samples plot above the general correlation line.

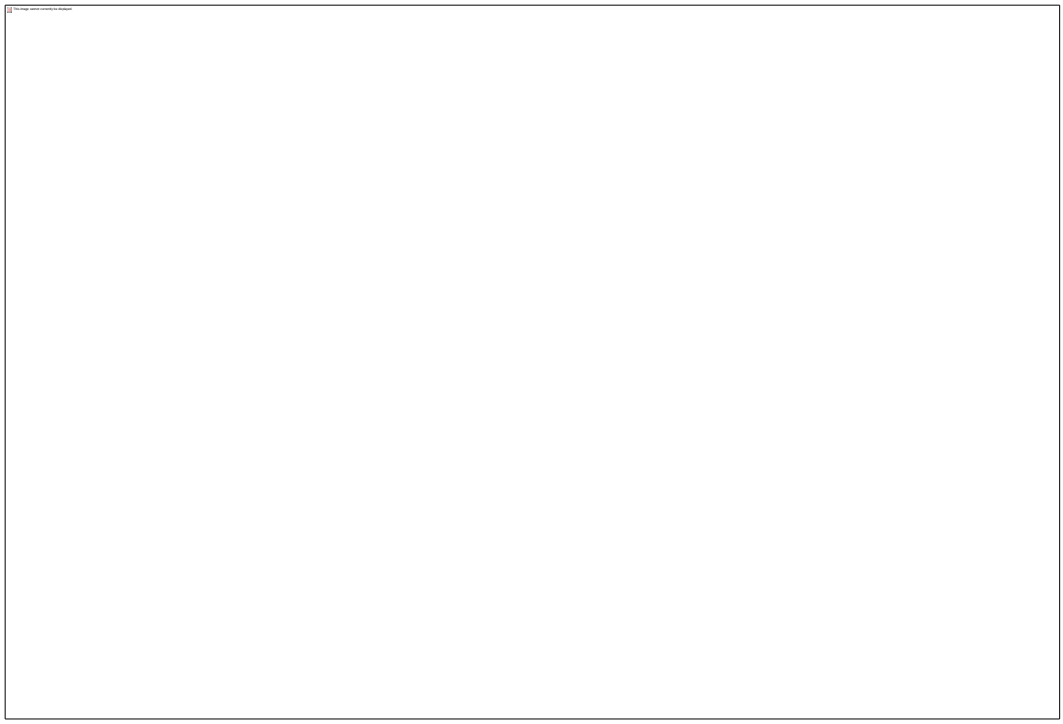

Figure 3-18 Major element cross-plots for the Teague 1-14H core: (A) %Si *versus* %Al; (B) %Ca *versus* %Al; (C) %K *versus* %Al; (D) %P *versus* %Al; (E) %Ti *versus* %Al; (F) %Fe *versus* %Al

Figure 3-19 shows a cross-plot of %Fe *versus* %S. Overlain are four trend lines representing the degree of pyritization (DOP), as previously discussed (Levanthal, 1979; Raiswell et al, 1988; Robinson, 2012). There is a general trend observed along the pyrite line, but significant scatter is also observed, especially at lower Fe and S concentrations. Samples from zone D (gray) show the strongest relationship to the DOP trend lines.

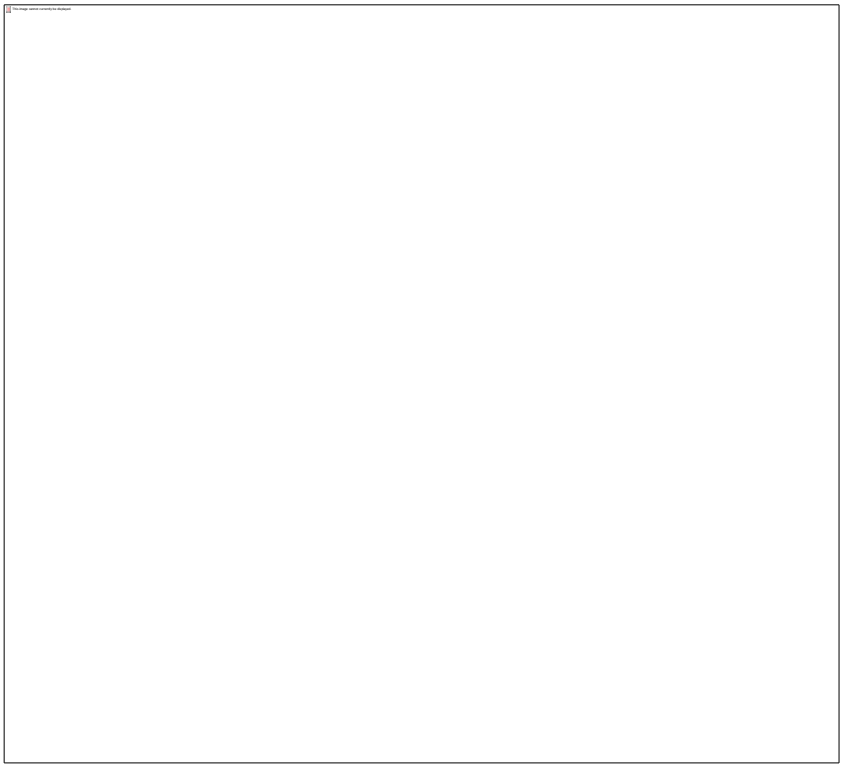

Figure 3-19 Cross-plot of %Fe versus %S for the Teague 1-14H core

Figure 3-20 shows various trace element enrichment factors plotted by depth for the Teague 1-14H core. Trace elemental data was only collected from the dark gray and black shale portions of the core, from depth 10005 feet to the end of the core. Enrichment factors are used here to determine if a sample is enriched in a given trace

element relative to an average gray shale, as previously discussed (Wedepohl, 1971; Calvert and Pederson, 1993).

Most samples in the Teague 1-14H core are somewhat enriched in molybdenum, chromium, uranium, nickel, zinc, and copper (fig. 3-20). The small portion from zone B (black) that was analyzed for trace elements records some depletion in each of elements. The most significant trace element enrichment is observed at the top of zone C (green).

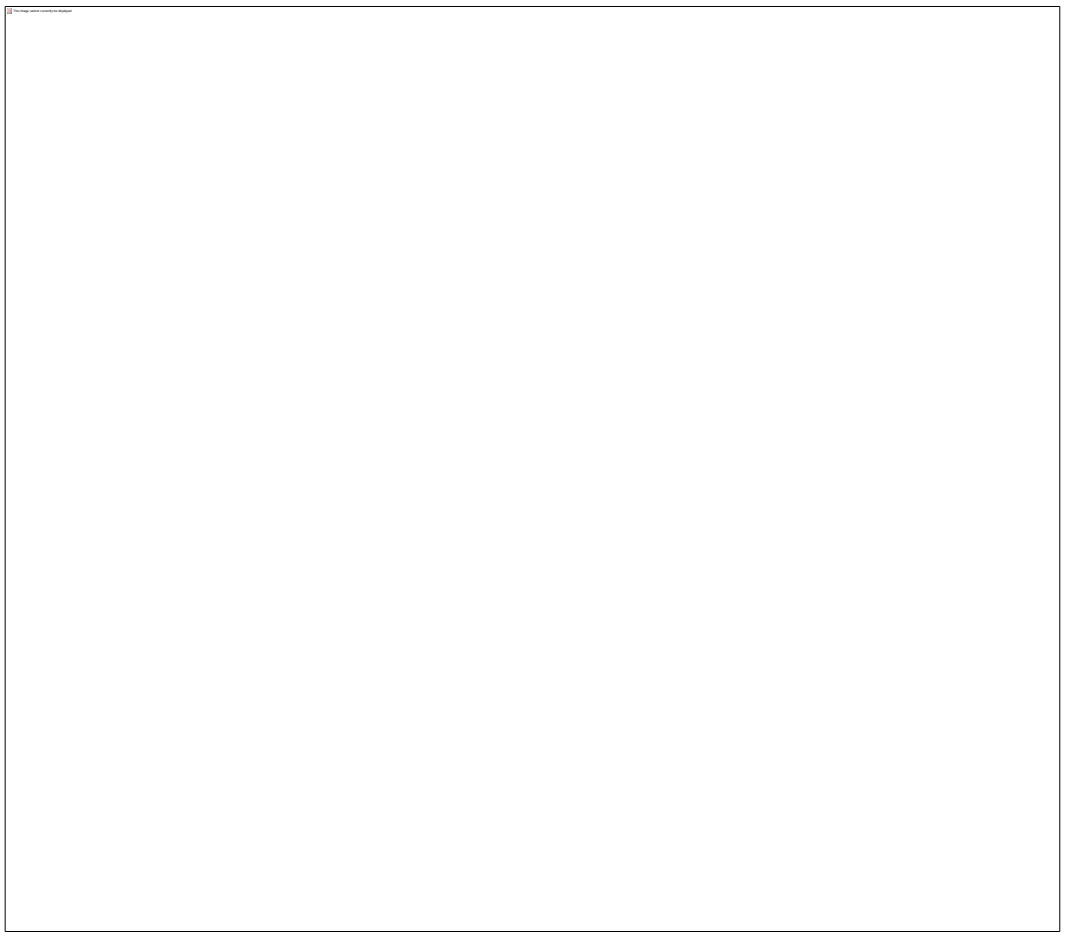

Figure 3-20 Down-core plot of the enrichment factors (EF) of Mo, Cr, U, Ni, Zn, and Cu for the Teague 1-14H core

Figure 3-21 shows the enrichment factor of manganese plotted by depth, as well as trace element ratios: Ni/Co, V/Cr, and V/(V+Ni) for the Teague 1-14H core. These ratios were chosen because they have been found to be indicative of paleoredox conditions, as previously discussed (Hatch and Leventhal, 1992; Jones and Manning, 1994; Rimmer, 2003). The enrichment factor of manganese is shown because it can also be used as an indicator of paleoredox conditions and longevity (Calvert and Pederson, 1993). It should be noted that some samples with ratios of very high or low magnitude were excluded in order to provide better resolution for the general population of samples.

The majority of the samples from zone A (red) of the Teague 1-14H core show some Mn enrichment. Samples from zones B and C (black and green) oscillate between Mn enrichment and depletion. Sample from zone D (gray) record Mn depletion. The highest overall magnitude for each of the trace element ratios are observed in zone C (green) of the Teague 1-14H core.

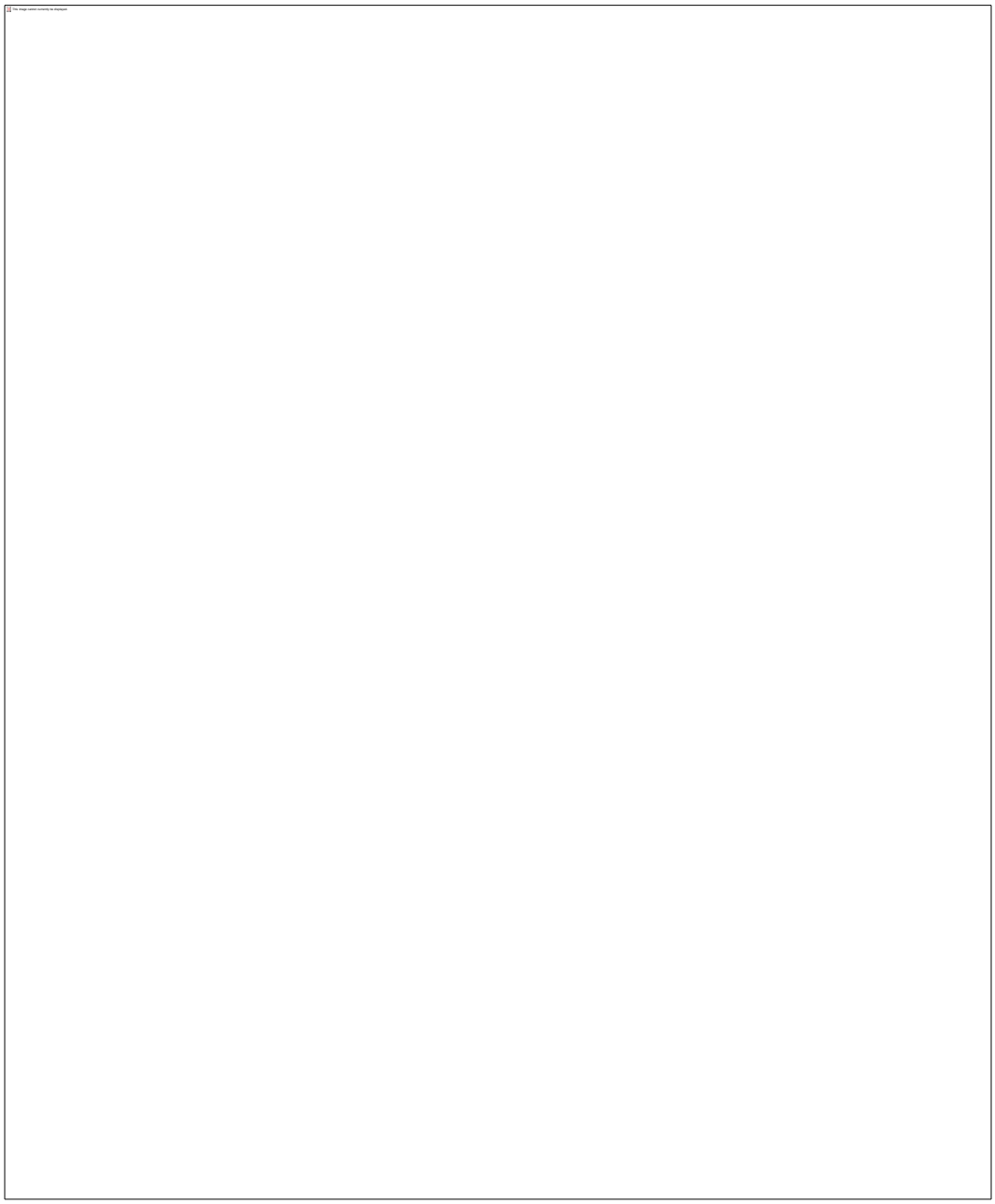

Figure 3-21 Down-core plot of EF Mn, Ni/Co, V/Cr, and V/(V+Ni) for the Teague 1-14H core

Chapter 4

Discussion

Bulk Geochemistry

The bulk geochemistry of each of the three cores studied provides insight into the general mineralogy of the Woodford formation in different areas of the Anadarko basin. Clay-calcite-quartz ternary diagrams depict, in general, a siliceous mudstone throughout the basin, with more calcium input to the north (fig. 3-3, 3-10, 3-17). The southernmost core studied, the Shi Randall 4-29H shows the most siliceous input of the three core, with few carbonate influxes (fig. 3-3). The Ridenour 1-20H core shows less silica dilution than the Shi Randall core, still with very few carbonate influxes (fig. 3-10). The Teague 1-14H core shows significant calcium dilution, specifically in zones A (red) and B (black), with significant siliceous input in zones C (green) and D (gray). The Teague 1-14H core lies on the edge of the basin, and may have been deposited in slightly shallower waters where carbonate was more readily deposited.

Major Elements

As previously discussed, Si, Ca, and Al can be used as proxies for quartz, calcite, and clay, respectively. By examining cross-plots of various major elements *versus* Al, the relationship of those elements to the clay mineral fraction of the sample can be inferred. A negative linear trend is observed between Si and Al for each of the cores studied (fig. 3-4A, 3-11A, 3-18A). This inverse relationship suggests that the clay fraction is diluted by the siliceous input. It is not possible to determine if this silica is biogenic or detrital from this data; however, previous studies suggest this is biogenic silica (Cardott, 2013).

Both Ti *versus* Al and K *versus* Al depict a strong positive linear correlations (Fig 3-4 C & E, 3-11 C & E, 3-18 C & E). This relationship indicated Ti and K are associated with the clay mineral phase. Ti is also an indicator of terrigenous sedimentations.

The cross-plot of iron *versus* aluminum shows a very weak positive trend in the Shi Randall 4-29H core (fig. 3-4F), and a stronger positive correlations in the Ridenour 1-20H and Teague 1-14H cores (fig. 3-11F, 3-18F). A strong correlations indicated most of the iron is in the clay fraction of the sample. Any samples that plot above the general trend line indicate iron present in a mineral phase other than clay (e.g. pyrite). Pyrite was observed in the cores during analysis, with the most pyrite being observed in the Shi Randall 4-29H core.

Degree of Pyritization

The iron *versus* sulfur cross-plot can be used to visually estimate the degree of pyritization (DOP) (fig. 3-5, 3-12, 3-19). The Shi Randall 4029H core shows two main trends, one along the “pyrite line” (DOP=1.0), and another along the DOP=0.25 line. The majority of the samples from zones A, B, and C plot along the “pyrite line”. This indicated that most of the sulfur in the system at the time of deposition went into pyrite. The samples from zones D and E that plot along the DOP=0.25 line suggest there was a lack of available sulfur to fully pyritize the available iron. Several samples from zones A and B plot above the “pyrite line” indicating pyrite formation was iron-limited. Other studies have shown sulfur to be adsorbed in organic material in iron-limited environments (Damste et al, 1990). Further study of the organic matter in the Woodford Shale is required to support this.

Trace Elements

Various trace elements can be used as indicators of paleoredox conditions. These trace elements are deposited as components of pyrite and organic matter, or as

distinct sulfide phases (Pratt and Davis, 1992; Wignall, 1994; Rimmer, 2003). Trace elements included in this discussion are Mo, Cr, U, Ni, Zn, and Cu. Also included in the discussion is the minor element, Mn, due to its paleoredox sensitivity.

The Shi Randall 4-29H core shows significant enrichment in each trace element studied (fig. 3-6), except for the samples from zone D (gray). Zone B (black) records significantly less trace element enrichment than zones A (red), C (green), or E (blue). Fluctuations in the enrichment of these trace elements generally coincide. Molybdenum is often considered one of the most diagnostic trace elements for sea-water reducing depositional environments (Dean et al, 1997; Rimmer, 2003) because it is highly enriched in modern-day sediments from reducing environments with free H_2S, such as the Black Sea and the Saanich Inlet (Crusius et al, 1996; Rimmer, 2003; Rowe et al, 2008). Mo in the Shi Randall 4-29H core is most enriched in the upper part of zone A (red) and the lower part of zone C (green). Enrichment of Mo, as well as Cr, U, Ni, Zn, and Cu, indicate euxinic or anoxic conditions during deposition of zone A (red), zone C (green), and zone E (blue). Zone B (black) possibly fluctuates between euxinic or anoxic conditions and dysoxic conditions. Zone D (gray) was likely deposited during oxic conditions due to the lack of enrichment of any trace elements.

The Ridenour 1-20H core also shows enrichment in Mo, Cr, U, Ni, Zn, and Cu (fig. 3-13). The highest enrichment of trace elements occurs in zone A (red), the bottom of zone B (black), and in the bottom half of zone C (green). It appears that an event occurred at the boundary of zone C (green) and zone B (black), causing an anoxic event that slowly became more oxic as zone B (black) was being deposited. Most of the Ridenour 1-20H core appears to have been deposited under anoxic or euxinic conditions, except for a section of zone C (green) that fluctuates between enrichment and depletion of these trace elements.

The Teague 1-14H shows enrichment in Mo, Cr, Ni, Zn, and Cu in zones C (green) and D (gray), with more enrichment in zone C (fig. 3-20). Less enrichment is seen in the Teague 1-14H core than in the Shi Randall 4-29H and Ridenour 1-20H cores. This is likely due to the core being taken from the edge of the basin, where there may have been shallower waters during deposition.

Manganese is indicative of paleoredox conditions because of the highly insoluble manganese oxides formed under oxic conditions (Calvert and Pederson, 1993). Figures 3-7, 3-14, and 3-21 show the enrichment factor of Mn plotted by depth for the Shi Randall 4-29H, Ridenour 1-20H, and Teague 1-14H cores, respectively. The background of these graphs are color coded to indicate oxic (blue), and anoxic (red) conditions. Enrichment in Mn occurs in sediments during oxic events, were as depletion occurs when oxygen is not readily available. The Shi Randall 4-29 core shows high frequency oscillations between Mn enrichment and depletion, with the exception of zone D (gray), which shows depletion of Mn (fig. 3-7). This oscillatory pattern indicates that periods of anoxia and euxinia were relatively short lived. However, due to the general enrichment of redox-sensitive trace elements, it can be inferred that significant sedimentation occurred during these anoxic or euxinic periods. The Ridenour 1-20H core shows significantly less variability in Mn enrichment than the Shi Randall 4-29H core (fig. 3-14). The majority of the samples are Mn depleted, indicating long periods of anoxia or euxinia. The upper portion of zone A (red), where some of the most trace element enriched samples are has several samples enriched in Mn, indicating oscillation between anoxic and oxic conditions. The Teague 1-14H core shows overall Mn enrichment in zone A (red) and zone B (black), an oscillatory pattern in zone C (green), and Mn depletion in zone D (gray) (fig. 3-21). This indicates anoxic conditions in zone D, oscillation between oxic and anoxic conditions in zone C, and generally oxic conditions in zones A and B. Oxic conditions are expected in zones A

and B of the Teague 1-14H core due to the abundance of carbonate in the samples (fig. 3-15, 3-17).

Several trace element ratios have previously been used as paleoredox indicators: Ni/Co, V/Cr, and V/(V+Ni) (Dypvik, 1984; Dill, 1986; Hatch and Leventhal, 1992; Jones and Manning, 1994; Rimmer, 2003). The thresholds for these ratios indicative of various paleoredox conditions are listed in Table 1. In both the Ridenour 1-20H core (fig. 3-14) and the Teague 1-14H core (fig. 3-21), Ni/Co and V/Cr appear to agree quite well. V/(V+Ni) shows generally the same trend as Ni/Co and V/Cr, however, most samples lie in the dysoxic to anoxic classification, where Ni/Co and V/Cr show more variation. Based on the Ni/Co and V/Cr ratios, it can be assumed that zone C (green) of the Ridenour 1-20H core (fig. 3-14) transitioned, from bottom to top, from oxic conditions, to anoxic conditions, followed by another cycle of oxicity and anoxia. Periods of dysoxia are recorded during the transitions from oxic to anoxic and back. Zone B (black) of the Ridenour 1-20H core was primarily deposited during dysoxic to oxic conditions. Zone A (red) of the Ridenour 1-20H core was deposited primarily during dysoxic to anoxic conditions.

It is suggested that zone D (gray) of the Teague 1-14H core was deposited under dysoxic to anoxic conditions, based on Ni/Co and V/Cr ratios (fig. 3-21). Zone C (green) of the Teague 1-14H core appears to have been deposited under primarily dysoxic to anoxic conditions, with some short-lived periods of oxicity.

The Shi Randall 4-29H core shows very high variability in Ni/Co and V/(V+Ni) ratios, from highly anoxic to oxic or dysoxic (fig. 3-7). This variability reinforces the oscillatory paleoredox conditions, as indicated by Mn enrichment (fig. 3-7). The V/Cr ratio for the Shi Randall 4-29H core shows significantly less variability than the other ratios. However, the majority of the samples oscillate between oxic and dysoxic conditions. The

bottom half of zone C (green) and the top portion of zone A (red) reveal periods of highly anoxic conditions, based on the V/Cr ratio. The V/(V+Ni) ratio indicates that the topmost portion of Zone A (red) was deposited under fairly stable euxinic conditions.

Chapter 5

Conclusions

Chemostratigraphy of the Woodford Shale of the Anadarko Basin was constructed using geochemical data collected by ED-XRF. Three cores were studied, the Shi Randall 4-29H, the Ridenour 1-20H, and the Teague 1-14H. The geochemical data and chemostratigraphy was used to draw conclusions about the depositional environment.

1. The Woodford Shale is a siliceous mudstone. The southernmost core, the Shi Randall 4-29H, contained the most silica of the three cores. Silica enrichment decreased to the north, with less silica input in the Ridenour 1-20 core and the least amount of silica enrichment in the Teague 1-14H core.
2. The relationship between iron and sulfur indicates significant pyritization of iron, which is supported by observation of pyrite in the cores. However, in the Shi Randall 4-29H core, iron appears to be the limiting agent of pyrite formation in the uppermost portion of the Woodford Shale.
3. Trace element enrichment indicates that the Woodford Shale was deposited under suboxic to anoxic or euxinic conditions. However, Mn enrichment suggests relatively short-lived periods of anoxia, fluctuating with periods of oxic bottom waters.

References

Amsden, T. (1975). Hunton group (Late Ordovician, Silurian, and early Devonian) in the Anadarko Basin of Oklahoma. *Oklahoma Geological Survey Bulletin 121*, 121-214.

Arthur, J. K., & Sageman, B. B. (1994). Marine black shales: depositional mechanisms and environments of ancient deposits. *Annual Reviews in Earth and Planetary Science*, 499-551.

Blackford, M. A. (2007). *Electrostratigraphy, Thickness, and Petrophysical Evaluation of the Woodford Shale, Arkoma Basin, Oklahoma.* Oklahoma State University.

Blakey, R. (2013, July). *Paleogeographic maps*. Retrieved from Colorado Plateau Geosystems, Inc.: http://cpgeosystems.com/paleomaps.html

Blatt, H. (1970). Determination of mean sediment thickness in the crust: a sedimentologic method. *Geologic Society of America*, 255-262.

Brown, D. (2008, July). Big Potential Boosts the Woodford. *AAPG Explorer*.

Buckner, N., Slatt, R. M., Coffey, B., & Davis, R. J. (2008). Stratigraphy of the Woodford Shale from Behind-Outcrop Drilling, Logging, and Coring. *AAPG Annual Convention.* San Antonio: AAPG.

Caldwell, C. (2012). Rock Types and lithostratigraphy of the Devonian Woodford Shale, Anadarko Basin, West-Central Oklahoma. *AAPG Annual Convention and Exhibition.* Long Beach: AAPG.

Calvert, S. E., & Pederson, T. F. (1993). Geochemistry of recent oxic and anoxic marine sediments: implications for the geological redord. *Marine Geology*, 67-88.

Cardott, B. (2013, April 11). Woodford Shale: from hydrocarbon source rock to reservoir. *AAPG Woodford Shale Forum*.

Cardott, B. J., & Lambert, M. W. (1985). Thermal Maturations by Vitrinite Reflectance of Woodford Shale, Anadarko Basin, Oklahoma. *The American Association of Petroleum Geologists Bulletin*.

Continental Resources. (2012, June). *Anadarko Woodford: Continental Resources*. Retrieved April 23, 2013, from Continental Resources Web Site: http://www.contres.com/operations/anadarko-woodford

Crusius, J., Calvert, S., Pederson, T., & Sage, D. (1996). Rhenium and molybdenum enrichments in sediments as indicators of oxic, suboxic, and sulfidic conditions of deposition. *Earth Planet Science Letters*, 65-78.

Curtis, M. E., Cardott, B. J., Sondergeld, C. H., & Rai, C. S. (2012). Development of Organic Porosity in the Woodford Shale with Increasing Thermal Maturity. *International Journal of Coal Geology*, 26-31.

Dean, W., Gardener, J., & Piper, D. (1997). Inorganic geochemical indicators of glacial-interglacial changes in productivity and anoxia on the California continental margin. *Geochim. Cosmochim. Acta.*, 4507-4518.

DeCelles, P., & Giles, K. (1996). Foreland basin systems. *Basin Research*, pp. 105-123.

Dill, H. (1986). Metallogenesis of early Paleozoic graptolite shales from the Graefenthal Horst (Northern Bavaria-Federal Republic of Germany). *Econ. Geol.*, 889-903.

Dypvik, H. (1984). Geochemical compositions and depositional conditions of upper Jurassic and lower cretaceous Yorkshire clays. *England Geol. Mag.*, 489-504.

Franseen, E., Byrnes, A., Cansler, J., Steinhauff, D., & Carr, T. (2004). The geology of Kansas Arbuckle Group. *Kansas Geological Survey*.

Gupta, N. (2012). *Multi-Scale Characterization of the Woodford Shale in West-Central Oklahoma: From Scanning Electron Microscope to 3D Seismic.* University of Oklahoma.

Hatch, J., & Leventhal, J. (1992). Relationship between inferred redox potential of the depositional environment and the geochemistry of the Upper Pennsylvania (Missourian) stak shale member of the Dennis Limestone, Wabaunsee County, Kansas, USA. *Chem. Geol.*, 65-82.

Hester, T., Schmoker, J., & Sahl, H. (1990). *Log-Derived Regional Source-rock Characteristics of the Woodford Shale, Anadarko Basin, Oklahoma.*

Hoffman, P. F., Dewey, J. F., & and Burke, K. (1974). Aulacogens and their genetic relationship to geosynclines with a Proterozoic example from the Great Slave Lake, Canada. In R. H. Dott, & R. H. Shaver, *Modern and ancient geosynclineal sedimentation: Society of Economic Paleontologists and Mineralogists Special Publication 19* (pp. 38-55).

Johnson, K. (1989). Geologic setting of the Arbuckle Group in Okalhoma. *Oklahoma Geological Survey Special Publication*.

Jones, B., & Manning, D. (1994). Comparison of geochemical indices used for the interpretation of paleoredox conditions in ancient mudstones. *Chem. Geol.*, 111-129.

Kluth, C. (1996). Plate tectonics of the Ancestral Rocky Mountains. In J. Johnson, *Paleotectonics and Sedimentation in the Rocky Mountains, United States: American Association of Petroleum Geologists, Memoir 41* (pp. 353-369).

Kuykendall, M., & Fritz, R. (2001). Misener Sandstone of Oklahoma. *AAPG Search and Discovery*, 117-134.

Leventhal, J. (1983). An interpretation of carbon and sulfur relationships in Black Sea sediments as indicators of encironments of deposition. *Geochim. Cosmochim. Acta.*, 133-137.

Over, D., & Barrick, J. (1990). The Devonian/Carboniferous boundary in the Woodford Shale, Lawrence uplift, south-central Oklahoma. In S. Ritter, *Early to middle Paleozoic conodont biostratigraphy of the Arbuckle Mountains, southern Oklahoma: OGS Guidebook 27* (pp. 63-73).

Pathi, V. S. (2008). *Factors Affecting the Permeability of Gas Shales.* Vancouver: The University of British Columbia.

Piper, D., & Calvert, S. (1009). A marine biogeochemical perspective on black shale deposition. *Earth Science Reviews*, 63-96.

Pompeck, J. (1901). Die Jura-Ablagerungen zqischem Regensburg and Regenstauf. *Geognistische Jahreshefte*, 139-220.

Potter, P., Maynard, J., & Pryor, W. (1980). *Sedimentology of Shale.* New York: Springer Verlah.

Pratt, L., & Davis, C. (1992). Intertwined fates of metals, sulfur, and organic carbon in black shales. In L. Pratt, J. Comer, & S. Brassell, *Geochemistry of Organic Matter in Sediments and Sedimentary Rocks* (pp. 1-27).

Raiswell, R., Buckley, F., Berner, R., & Anderson, T. (1988). Degree of pyritization of iron as a paleoenvironmental indicator of bottom-water oxygenation. *J. Sediment. Petrol.*, 812-819.

Redden, J. (2013, January). Woodford Shale: SCOOP Helps Advance Oklahoma's Drive for Oil. *World Oil*.

Rimmer, S. (2004). Geochemical paleoredox indicators in Devonian-Mississippian black shales, Central Appalachian Basin (USA). *Chemical Geology*, 373-391.

Roberts, C. (1988). Laminated black shale-chert cyclicity in the Woodford Formation (Upper Devonian of southern mid-Continent). *Univ. of Texas at Dallas, unpublished M.S. thesis*.

Rose, K., Douds, A., Pancake, J., Pratt III, H., & Boswell, R. (2004). Assessing subeconomic natural gas resources in the Anadarko and Uinta Basins. *AAPG Annual Concention*.

Rowe, H. D., Hughes, N., & Robinson, K. (2012). The quantification and application of handheld energy-dispersive x-ray fluorescence in mudrock chemostratigraphy and geochemistry. *Chemical Geology*, 122-131.

Schieber, J., & Zimmerle, W. (1998). Introduction and overview: the history and promis of shale research. In J. Schieber, W. Zimmerle, & P. Sethi, *Shales and Mudstones* (pp. 1-10). Stuttgart: Schweizerhbart'sche Verlagsbuchhandlung.

Schmoker, J. (1981). Determination of organic-matter content of Appalachian Devonian shales from gamma-ray logs. *AAPG Bulletin*, 1285-1298.

Slatt, R. M., & O'Brien, N. R. (2011). Pore Types in the Barnett and Woodford Gas Shales: Contribution to Understanding Gas Storage and Migration Pathways in Fine-Grained Rocks. *AAPG Bulletin*, 2017-2030.

Tarr, R. (1955). Paleogeologic map at base of Woodford, and Hunton isopachous map of Oklahoma. *AAPG*.

U.S. Energy Information Administration. (2011). *Lower 48 States Shale Plays.*

Varacchi, B. H. (2011). *Rock Physics and Mechanical Stratigraphy of the Woodford Shale, Anadarko Basin, Oklahoma.* Oklahoma State University.

Vulgamore, T., Wolhart, S., Mayerhofer, M., Clawson, T., & Pope, C. (2008, March). Hydraulic Fracture Diagnostics Help Optimize Stimulations of Woodford Shale Horizontals. *American Oil and Gas Reporter*.

Watson, B. P. (2008). *Internal Stratigraphy, Composition, and Deposition Setting of the Woodford Shale in Southern Seminole County, Oklahoma.* Oklahoma State University.

Wedepohl, K. (1971). Environmental influences on the chemical composition of shales and clays. In L. Ahrens, F. Press, S. Runcorn, & H. Urey, *Physics and Chemistry of the Earth, vol. 8* (pp. 307-331). Oxford: Pergamon.

Wicker, J. M. (2008). *Lithologic and Geochemical Assesment of the Hydrocarbon Producing capability of the Woodford Shale in Southern Oklahoma.* Oklahoma State University.

Wignall, P. (1994). *Black Shlaes.* Oxford: Clarendon Press.

Biographical Information

After graduating high school, Karen McCreight obtained an associate degree at Tarrant County College. She started her education at University of Texas at Arlington in the fall of 2010. Karen started at UTA as a chemistry major, but quickly determined geology was the science for her. Karen was privileged to meet Dr. Harry Rowe while changing my major and started working in his geochemistry research group. She has been able to do geochemical research and chemostratigraphy of the Wolfcamp formation, the Barnett formation, and the Woodford formation. Karen plans to use her knowledge of the geochemistry of black shales to obtain a career in the oil and gas industry.